# Iron-Impregnated Nanosized Silica and Alumina: Implications for Contaminant Transformation

by

Yue Li, B.S.

A Thesis

In

Civil Engineering

Submitted to the Graduate Faculty
of Texas Tech University in
Partial Fulfillment of
the Requirements for
the Degree of

Master of Science
in
Civil Engineering

Approved

Dr. Weile Yan
Chair of Committee

Dr. Moira K. Ridley

Dr. W. Andrew Jackson

Mark Sheridan
Dean of the Graduate School

December, 2014

# Acknowledgements

Upon accomplishing this thesis, I would like to thank the patient instructions and insightful guides given by my research advisor Dr. Weile Yan. Her concrete faith on the topic always gave me courage in the thorny way of research, and her persistence on perfection always influences me on my own exploration for the research. I also would like to thank my committee member Dr. Moira Ridley and Dr. Andrew Jackson for their time and valuable feedback on this thesis. I appreciate Dr. Ridley for her professional and confident advice. I also thank Dr. Jackson for his perceptive opinions on the research. Additionally, I would like to thank the Lab manager Mr. Brad Thornhill in Department of Civil and Environmental Engineering, and Dr. Juliusz Warzywoda in Materials Characterization Center for their consistent help in the labs. I also would like to thank the TAs, RAs working in the same labs for sharing, helping and supporting.

At last, I would like send sincere appreciation for my parents, for their firm support when things were tough and for their selfless love that has been always my encouragement.

# Contents

# Abstract

Aqueous iron and prevailing mineral oxides such as silicon and alumina interact to create a vast amount of iron-enriched surfaces with considerable surface adsorption capacity and redox activity in the natural environment. Considering the abundance and benign nature of these oxides and also the significant role of iron in both adsorption and redox transformation, iron-immobilized silica and alumina are of great interest in the field of recalcitrant contaminant transformation. In this study, nanoscale silica aerogel and alumina aerogel which act as proxies of colloidal silica and alumina solid phase were impregnated with low concentrations of iron by immersing them into dilute aqueous solutions of Fe(II) or Fe(III) ions. The resultant solid phases were investigated for catalytic activity and adsorption potential with benzoate as the probe compound. Both impregnated solids can catalyze Fenton-like reactions in the presence of hydrogen peroxide. pH is influential in Fenton-like reactions that are catalyzed by the impregnated solids, and benzoate transformation can be hindered by the catalytic failure to generate hydroxyl radicals in neutral and alkaline conditions. The structure of interfacial iron species after impregnated with ferrous precursor includes isolated Fe, ferric oligomers and big precipitates of ferric oxides, whereas configuration of impregnation resulted ferric precursor contains primarily ferric oligomer and precipitate. Among three types of impregnation, isolated Fe and oligomers are good catalysts for Fenton reactions, yet big precipitates are good adsorbents. Silica as a substrate promotes isolated-iron-type impregnation, while alumina prefers formation of oligomers.

# List of Tables

# List of Figures

# Chapter 1

# Introduction

## 1.1. Environmental chemistry of iron species

The interactions between iron species and natural minerals have been under intense study in the recent decades. The continuous attention is not only due to the abundance of iron on Earth and its participation in a wide variety of geochemical transformations but also the strong anthropogenic input in the redistribution of iron species in the natural environment, which brings a net accumulation of iron oxides along with natural processes such as mineral erosion and weathering.

### 1.1.1. Iron species in aqueous phase

Iron has two major oxidation states, the divalent iron (also referred to as ferrous iron) and trivalent iron (referred to as ferric iron), and iron switches between these two states during its participation in natural processes such as adsorption/precipitation and redox transformation. Ferrous iron can be easily oxidized to ferric iron in the presence of dissolved oxygen (Singer & Stumm, 1970; Sung & Morgan, 1980). Both ferrous and ferric ions are subject to hydrolysis when they are in contact with aqueous solution, and the hydrolysis become stronger when the amount of hydroxide ions ($OH^-$) increases in solution, that is to say, when the pH of the aqueous solution increases. Equations 1.1 and 1.2 show processes of ferrous and ferric hydrolysis. Ferrous salts are soluble at up to

neutral pH values, mainly in a hexa-aquo form ($Fe(H_2O)_6^{2+}$), if they are not complexed with $OH^-$ when pH is above 3 (Pignatello *et al.*, 2006). Ferric iron exists as the hexa-aquo ion, $Fe(H_2O)_6^{3+}$, in a strictly acidic environment containing only the non-complexing counterions, namely, $ClO_4^-$ and $NO_3^-$. Hydrolysis of ferric iron occurs readily when pH is above three following Equation 1.2 (Pignatello *et al.*, 2006). All the hydrolyzed products of Fe(III) have low solubility in aqueous solution, and thus olation and oxolation of them take place to create poly-nuclear iron complexes. These complexes eventually form precipitates from aqueous solution which are defined as iron (oxyhydr)oxides. These ferric oxides (including ferric oxide with oxygen bond, ferric hydroxide with $OH^-$, and ferric oxyhydroxide) can co-precipitate aqueous Fe(II) ions under certain conditions, and the co-precipitation results in formation of Fe(II)-Fe(III) oxides (Larese-Casanova *et al.*, 2012). A higher aqueous iron concentration is found in reducing environments such as groundwater where ferrous iron dominates, and the scarcity of soluble iron yet the ubiquitous occurrence of iron-containing minerals in neutral and alkaline environments is attributed to the low solubility of both iron species under these environments. Hypervalent iron, including Ferryl or Fe(IV) species among others, has also been shown to be formed under certain conditions during the Fenton process (J. L. Wang & Xu, 2012). The Fenton process refers to a series of cyclic reactions between hydrogen peroxide and iron species involving the generation of multiple radicals as will be reviewed in the following sections. However, iron in this oxidation state is not typically found in natural environments.

$$Fe(H_2O)_6^{2+} + H_2O \leftrightarrow Fe(H_2O)_5OH^+ + H_3O^+ \qquad (1.1a)$$ (Wells & Salam, 1965)

$$Fe(H_2O)_6{}^{2+} + 2H_2O \leftrightarrow Fe(H_2O)_4(OH)_2 + 2H_3O^+ \quad (1.1b)$$ (Wells & Salam, 1968)

$$Fe^{3+} \leftrightarrow FeOH^{2+} \leftrightarrow Fe(OH)_2^+ \leftrightarrow Fe_2(OH)_2^{4+} \leftrightarrow other\ polynuclear\ species \leftrightarrow Fe_2O_3 \cdot nH_2O(s)$$

(1.2) (Pignatello *et al.*, 2006)

1.1.2. Behavior of iron species in heterogeneous precipitation

Oxygenation of Ferrous iron is controlled by the condition of the aqueous solution, such as partial pressure of dissolved oxygen, ionic strength and temperature (Sung & Morgan, 1980). While in natural environments, the presence of common mineral surfaces such as silica and aluminosilicates catalyzes the oxidation of Fe(II) to Fe(III) by dissolved oxygen (Stumm & Sulzberger, 1992). It is thought that oxidation is preceded by an adsorption step in which the ferrous iron adsorbs to mineral surfaces, and this adsorption step is assisted by surface hydroxyl groups which act as ligands that can complex with the ferrous iron to facilitate its conversion to the ferric iron (Wehrli *et al.*, 1989). Given the low solubility in aqueous solution that ferric compounds have, heterogeneously ferric precipitation, namely iron (hydr)oxides, occurs readily after the ferrous oxygenation catalyzed by mineral surfaces. The morphology of heterogeneously formed iron (hydr)oxides on the surface of a solid phase is a result of two competing processes: multilayer adsorption which results in a small cluster, and growth of the small cluster which gives rise to a big precipitate.

The development of surface ferric (hydr)oxide after the initial adsorption step (continuous multilayer adsorption or growth) is delicately controlled by the nature of the aqueous-solid system, namely electrostatic forces and the nature of the substrate (Hu *et al.*, 2013; Jun *et al.*, 2010). Electrostatic forces in the aqueous system execute their effects in multiple ways. For instance, electrostatic force creates surface free energy or interfacial tension among the interfaces, including the substrate-cluster/precipitate interface, cluster/precipitate-water interface and water-substrate interface. Controlling the pH of an aqueous solution away from the point of zero charge (pzc) of a metal oxide can alter the adsorption of protons on the surface, and thus raise the surface charge density, and thereupon decrease the surface free energy of the metal oxide. Enhanced ionic strength compresses the electrical double layer (a layer of electrons on the surface defined by the surface charge mainly caused by surface hydroxylation and the corresponding counterions) of a surface thereby allowing more sites to get charged, and then contributes to the lowering of interfacial tension (Vayssieres *et al.*, 2001). The development of surface iron (hydr)oxide is also affected by the structural matching between precipitate and substrate (Snoeyink & Jenkins, 1980). This is further proven by recent research. Hu *et al.* (2013) concluded both a high water-substrate interfacial energy and a low precipitate-substrate interfacial energy accelerate interaction between substrate and particles, resulting in a greater amount of small clusters than that of big precipitates. The structural mismatch, specifically metal-oxygen bond length mismatch, between the ferric (hydr)oxide and substrate affects precipitate-substrate interfacial energy.

### 1.1.3. Properties of iron oxides at solid-water interface

Both ferrous and ferric ions are coordinated with water molecules in aqueous solutions and are subject to hydrolysis when pH is near-neutral or alkaline as reviewed above. By the same token, the iron oxides are also complexed with hydroxyl groups in an aquatic environment. Hydrolysis of iron oxide is attributed to its surface acidity. Despite the prevailing existence of iron minerals in nature, iron oxides often exhibit a colloidal feature in aqueous solution (Cornell & Schwertmann, 2006). As a consequence of being colloidal particles, the surface to volume ratio of these iron oxides is high, which results in a substantial proportion of atoms exposed on the surface. Since the coordination environment of the surface atoms is not fully satisfied, surface Fe atoms can behave as Lewis acids, that is to say, as surface acids. Upon submerging in aqueous solutions, the surface of iron oxides will be covered with hydroxyl groups, a typical Lewis base, from water dissociation, and the hydroxyl ligands are in turn coordinated with the underlying iron atoms. The coordination of hydroxyl groups is followed by the buildup of water molecules via hydrogen bonds. The entities of adsorbed hydroxyl groups, that have double pairs of electrons and also dissociable protons, allow iron oxides to be amphoteric. In other words, iron oxides interact with both acids and bases.

## 1.2. Iron-based catalysts in natural and engineered aqueous environments

Homogeneous advanced oxidation processes have been widely used in the field of environmental cleanup for the degradation of recalcitrant organic pollutants such as

organic dyes and polyaromatic hydrocarbons and the sequestration of poisonous inorganic contaminants such as arsenic. Advanced oxidation processes (AOP) refer to the oxidative breakdown of the contaminants through the generation of strongly oxidizing radicals by radical-generating compounds such as ozone and hydrogen peroxide at ambient temperature or oxygen gas at a temperature often higher than 100℃, and such processes often require the use of ultraviolent irradiation and/or catalytic metal ions. However, the drawbacks of homogenous AOP reactions, including sludge production and requirements for acidification and neutralization of treated effluent, have shifted the attentions to heterogeneous AOP. Different types of catalysts for heterogeneous AOP processes will be discussed subsequently with a focus on the categories of materials relevant to this thesis.

### 1.2.1. Fe(II)/Fe(III)-catalyzed oxidative transformation of contaminants

The Fenton process refers to a series of cyclic reactions that take place homogeneously in acidic aqueous solution containing iron species, when hydrogen peroxide is used as an oxidant precursor. Table 1.1 indicates typical Fenton reactions. As a matter of fact, Fenton chemistry is among the most widely used iron-catalyzed reactions in environmental decontamination. To differentiate from ferrous iron-initiated reactions, the reactions occurring in a aqueous system where ferric iron initially exists are commonly called Fenton-like reactions, although the fundamental chemistry of radical formation and Fe(II)/Fe(III) redox cycling is essentially the same.

Table 1.1. Classic Fenton cyclic reactions (Pignatello *et al.*, 2006)

$$Fe(II) + H_2O_2 \rightarrow Fe(III) + OH^- + HO\cdot \quad (1.3.1)$$

$$Fe(III) + H_2O_2 \rightarrow Fe(II) + H^+ + HO_2\cdot \quad (1.3.2)$$

$$HO\cdot + H_2O_2 \rightarrow HO_2\cdot + H_2O \quad (1.3.3)$$

$$HO\cdot + Fe(II) \rightarrow Fe(III) + OH^- \quad (1.3.4)$$

$$Fe(III) + HO_2\cdot \rightarrow Fe(II) + O_2 + H^+ \quad (1.3.5)$$

$$Fe(II) + HO_2\cdot + H^+ \rightarrow Fe(III) + H_2O_2 \quad (1.3.6)$$

$$HO_2\cdot + HO_2\cdot \rightarrow H_2O_2 + O_2 \quad (1.3.7)$$

The effective species for degrading recalcitrant organics created in reactions above is hydroxyl radical (HO·), which has a strong but non-selective nature. Hydroxyl radicals can break down organic compounds via three typical pathways: hydrogen-abstraction, addition to carbon double bond, and addition to aromatic ring forming a hydroxycyclohexadienyl radical (Lal *et al.* (1997)) (refer to Scheme 1.1). Note that the third pathway is reversible. Though HO· is not selective, some organic compounds such as benzoate and formate react preferentially with hydroxyl radical over other oxidants, and these chemicals are widely used as probe compounds or quenching agents for hydroxyl radicals (Baker and Gebicki (1984), Sutton (1985)).

Scheme 1.1. Generation of HO· by classic Fenton reaction and reactions with organic contaminants

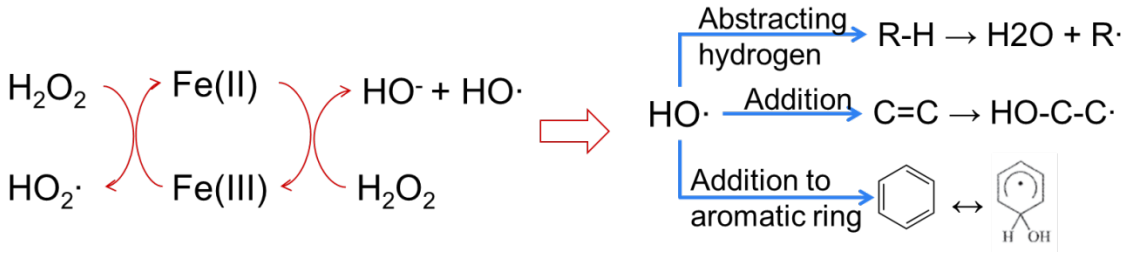


There is an ambiguity concerning the optimal pH for the homogeneous Fenton process. The kinetic rate of Fenton reactions is strongly dependent on pH because pH dictates the speciation of iron in the aqueous environment. J. L. Wang and Xu (2012) propose that the rate of ·OH generation reactions (Equation 1.3) reaches the highest at pH ~ 2.8, since there is a maximum amount of Fe(II) in the solution attained, and the presence of soluble Fe(III) around that pH. Whereas at higher pH values (pH >4), hydroxylation of ferric ion as well as precipitation of $Fe(OH)_3$ take place, and thus decrease in reaction rates is expected. Consequently, the optimum pH range for homogeneous Fenton reactions is 2-4. However, in another review (Pignatello *et al.* (2006)) it is argued that $Fe(OH)_2$, which dominants over all the other ferrous species at pH ~ 4, is "10 times more reactive" than Fe(II) and contributes to highest catalytic rate at pH ~ 4. The *apparent* best pH observed in actual applications is due to the solubility of Fe(III) species rather than that of Fe(II). Note that the significance of pH effect varies with the nature of the contaminants being oxidized. For aromatic compounds, such as phenol and benzoate, oxidation is only observed in acidic environment. However, for methanol, Reactive Black 5 (an azo-dye), and arsenite, certain degree of oxidation is detected at neutral to alkaline pHs, and the

oxidants formed under these conditions are postulated to be high-valent metal complexes of iron, i.e. ferryl (Fe (IV)) complexes.

### 1.2.2. Main types of catalysts

#### *1.2.2.1. Iron oxides*

The removal of arsenic from drinking water by iron (hydr)oxide has been continuously studied since effective adsorption of both As(III) and As(V) to iron oxides and co-precipitation (Meng *et al.* (2001)) are observed with arsenic at environmentally-relevant concentration levels. The efficacy obtained is explained to be a result of strong interaction between iron and arsenic (such as formation of inner-sphere complexes). It is discovered that in the As-Fe interaction there is a stronger binding of As(V) to iron oxides than that of the more toxic trivalent form As(III), and based on this nature of As species many researches have proposed that the pre-oxidation of As(III) to As(V) is a solution to achieve higher removal of arsenic. A promising method for pre-oxidation is the application of AOP processes with iron-containing minerals (Gupta *et al.*, 2005; Joshi & Chaudhuri, 1996; Thirunavukkarasu *et al.*, 2003) (see the following content).

#### *1.2.2.2. Iron-containing minerals*

The catalytic ability of common minerals that contains Fe(II) or Fe(III) have been studied because of their natural abundance, and also the low solubility that those minerals have in natural aqueous environment with neutral pHs, which qualifies them to be heterogeneous catalysts in the neutral environment. Studies investigating goethite, hematite, magnetite,

ferrihydrite, pyrite and lepidocrocite have deepened our understanding of the role of iron in the oxidation of organic compounds. Matta *et al.* (2007) concluded that the available soluble iron content and the fraction of desorbed contaminants from clay minerals both control the reaction rates in oxidation processes. It is also noted that Fe(II)-bearing minerals are more reactive than Fe(III)-bearing minerals on degrading 2, 4, 6-trinitrotoluene (TNT) and generating hydroxyl radical (Kwan & Voelker, 2003). Yeh *et al.* (2008) observed varied removal efficiencies when different contaminants were oxidized under the same oxidative conditions where goethite was used as the catalyst. They reported that the presence of multiple pollutants can cause an effect on the degradation efficiency of each contaminant. The generation rate of HO· is proposed be proportional to the product of surface area of the catalyst and $H_2O_2$ concentration in the solution multiplied by a certain coordinating factor unique to a specific iron-containing mineral (Kwan & Voelker, 2003). While generation of HO· during formic acid degradation in well-controlled experiments can be successfully predicted by this model, the model tends to over-expect the amount of HO· generated for other cases. Both Liou and Lu (2008) and Barreiro *et al.* (2007) remarked on the importance of ambient pH on contaminant oxidation when they researched on goethite and ferrihydrite catalysts respectively, stressing the role of pH in controlling ferrous ion solubility, which in turn influences the classic HO· producing step (Table 1.1, eq 1.3.2). Note that scarcely any researchers have discussed in details the possible relationship between the reactivity of iron minerals and their particular structural features. Most consider the reactivity of iron-containing surfaces is directly correlated with the specific surface area (Hanna *et al.*, 2008; Poulton *et al.*, 2004).

*1.2.2.3. Iron-immobilized materials*

Interactions occurring between natural silicon-containing and aluminum-containing minerals and iron species are investigated and developed by scientists and engineers in recent decades (Ryan & Gschwend, 1994; H. Wang *et al.*, 1993), and consequently engineered iron-immobilized materials are initiated and attract increasing attention.

Iron-immobilized materials that are under investigations diverge into two categories: naturally existing materials (Zachara *et al.*, 1995; Zhang *et al.*, 2004) and engineered materials (González-Bahamón, Hoyos *et al.*, 2011; González-Bahamón, Mazille *et al.*, 2011). Different methodologies are reported to synthesize engineered iron-immobilized catalysts. Substrates include natural silicon/alumina containing materials (namely zeolites) and manufactured silica and alumina. Batch adsorption is mostly used for iron impregnation on surfaces under varied conditions, such as temperature, pH and different precursor concentration. Sometimes additional treatment such as calcination is used after synthesis when a certain probe compound is selected (Lund & Dumesic, 1981; Yuen *et al.*, 1982). Sol-gel method, which involves gelling, precipitating, and coating of metal oxides after hydrolysis-assisted polymerization, is also widely applied to generate nano-sized material with high specific surface area (Martinez *et al.*, 2007; Prakash *et al.*, 2004).

A vast amount of researches is assessing iron-immobilized catalysts' capacity as a sorbent, while the redox potential of the catalysts is also studied. Typically, coating of iron species on silica is proposed to increase the specific surface area compared to the

bulk substrate. Yet it is also reported that the surface charge of silica was changed to favor the adsorption of Nickle to the surface by the chemical forces created by iron coating (Xu & Axe, 2005). $Si^{4+}$ ion can coordinate into the tetrahedral sites of iron oxides due to the known tendency of Si atom for tetrahedral coordination as a result of "covalency and size consideration" (Lund & Dumesic, 1981). In terms of catalytic ability for redox reactions, the efficient utilization of $H_2O_2$ by iron-immobilized materials is argued to be a result of both a better dispersion of iron species on the surface of the substrate and an altered electrical property of the synthetized catalysts compared to the pristine materials, that is to say, a improved surface charge that attracts and pair the oxidant and contaminant on (circum)surface (Pham *et al.*, 2009).

## 1.3. Objectives on the study of iron impregnated solid phases

Interfacial iron species have a widespread existence in natural environments where solid-water interfaces dominant, such as oxic/anoxic transition zone, and this prevalent existence is ascribe to the surface-catalyzed ferrous oxygenation and low solubility that ferric compounds have in neutral and alkaline aqueous environment. Despite the extensive body of research on environmental significance of iron oxide in terms of its adsorption capacity (reviewed in Section 1.2.2), the chemistry and behavior of these interfacial iron species have not been systematically investigated. With its colloidal nature, iron impregnation on natural solid phases cam possibly enhance surface reactive site and alter electrostatic properties of the surface so that the iron-impregnated solids

favor more adsorption of contaminants. Another promising while not well-understood practice is the redox ability of the interfacial iron species relative to single-phase iron-oxide nanoparticles that are on the same dimensional level, taking into account that the substrate and the surficial transition metal species may interact to create a significant catalytic activity. In fact, studies have shown that neither silica nor alumina is catalytic-reactive when exposed to aqueous contaminants and oxidants, however, both degradation of compounds and generation of HO· are concretely observed when iron dispersed surfaces is used (Larese-Casanova *et al.*, 2010; Pham *et al.*, 2009). Owing to benefits brought by heterogeneous catalysts outlined above, it is quite worthy to systematically investigate the catalytic activity of iron-impregnated silica and alumina.

Specifically, the catalytic ability of iron-impregnated solid phases was assessed by examining effect of amount of iron impregnated, effect of precursors for impregnation, and effect of reacting pH on contaminant removal efficiencies. Amount of iron impregnated was controlled by altering the concentration of iron precursor in the solution for impregnation. Two different precursors were used, namely ferrous sulfate and ferric chloride which represent ferrous iron and ferric iron respectively. Secondly, influence that a substrate can have on interfacial iron structure was scoped by applying two distinct substrates, nano-sized aerosilica and nano-sized aeroalumina, that have divergent surface electrical features in similar pH range. At last, relationship between the structure of iron impregnation and the catalytic ability was discussed.

# Chapter 2

# Materials and Methods

## 2.1. Reagents

All the glassware and HDPE bottles employed in this study were soaked in 10% nitric acid for more than 24 hours to remove any residual impurities and rinsed with distilled deionized water (DDI) three times before usage. All solutions in adsorption and batch experiments were prepared from distilled deionized water (DDI) produced by a Milli-Q system (CFOF 01205, 1x Super-C Organics Removal Cartridge, 2x Ion-Ex Deionization Cartridges, 1x Organex-Q Trace Organic Removal Cartridge, 1x Millipak®-Filter Unit). All chemicals used in the laboratory study were either of ACS grade or analytical reagents. Ferric chloride hexahydrate ($FeCl_3 \cdot 6H_2O$), ferrous sulfate heptahydrate ($FeSO_4 \cdot 7H_2O$), hydrogen peroxide ($H_2O_2$, 3% w/w) and sodium benzoate ($C_7H_5O_2Na$) were purchased from Fisher Scientific. Aerogels of silica and alumina with low densities, high surface areas, and high porosity were obtained from Sigma-Aldrich. Buffering agents including 2-(N-morpholino) ethanesulfonic acid (MES), N-(2-hydroxyethyl)piperazine-N'-2-ethanesulfonic Acid (HEPES), 3-(N-morpholino)propanesulfonic acid (MOPS) were purchased from Acros Organics. In typical adsorption experiments, stock solutions of ferric chloride and ferrous sulfate were prepared below a concentration of 20 mM on the day of experiments. The stock solutions were used as-is without pre-acidification. MES, MOPS, HEPES buffers were prepared, titrated to predetermined pH values with 10%

(v/v) sodium hydroxide and 20% (v/v) hydrochloric acid, and let stabilized for at least 2 hours before use.

## 2.2. Surface characterization

Diffuse reflectance UV-Vis (DR UV-Vis) spectroscopy (Cary 5000 UV-Vis-NIR spectrophotometer) was employed to characterize the molecular structure of Fe on the substrate surface. A small amount (less than 100 mg) of the solid particles was placed into a Praying Mantis$^{TM}$ diffuse reflectance sample holder (Harrick Scientific products Incorporation) with repetitive compressing-filling-compressing steps until a smooth, flat surface parallel to the holder rim was created. Diffuse reflectance spectra are obtained by measuring the amount of radiation from light source reflected by the sample surface and compare that with the radiation reflected by a reference material, commonly known as a baseline. The baseline spectrum was collected for pristine silica or alumina, respectively. The raw data collected was in the form of percentage reflectance (%R) from 200 to 800 nm wavelength at a slow acquisition speed (1.5 nm/sec). The artifact in the spectra caused by a change of light source at transition wavelength of 350 nm was corrected by multiplying the %R values collected after the transition wavelength by a correction factor, which was calculated by dividing %R at 350 nm by %R at 349 nm. The %R data was converted to the Kubelka-Monk function, F(R), using Eq 4. Kubelka-Munk function relates diffuse reflectance to the ratio of absorption (amount of radiation absorbed by the sample) and the scattering (radiation reflected), so that it enhances absorption activity of the sample yet levels off the effect of light scattering.

$$F(R) = \frac{(1-R)^2}{2R} \quad (2.1)$$

## 2.3. Adsorption experiments

The impregnation of iron on silica and alumina followed a simple aqueous adsorption procedure (Table 2.1). To compare the effect of iron precursor on the structure and reactivity of the resultant iron-impregnated solids, two forms of iron solutions, prepared from ferrous sulfate and ferric chloride salts, respectively, were used in the adsorption experiments. The resultant particles were denoted Fe(II) or Fe(III) to reflect their starting valence states. For the preparation of Fe(III) initiated iron impregnated nano-silica and nano-alumina, 0.3 g pristine solid phases and 5 mL concentrated sodium chloride at 1 mole/L and a measured volume of Fe(III) stock solution (Table 2.1) were added into a 500 mL HDPE bottle sequentially and then the slurry was diluted to 500 mL with DDI water while pH was monitored but not controlled during the adsorption process over 24 hours. DDI water was used as produced, thus adsorption was operated in presence of dissolved oxygen. The sodium chloride background gave an ionic strength = 0.01 for all experiments while the initial Fe(II) concentration in solution was varied in the range of 0.01~1.6 mM. Adsorption was assisted by vigorously shaking with Lab companion SK-300 shake. After a 24-hour adsorption period and 12+/-2 hours for solids settling, the solution was filtered through 0.2 μm membrane filter (disposable syringe filter from Millipore (SLLG025SS, Hydrophilic, PTFE, 25 mm, ethylene oxide sterilized) and membrane filter from Pall Corporation (60301, Hydrophilic polyethersulfone)). The

filtrate was collected for analysis of total dissolved iron by atomic absorption spectroscopy (Perkin Elmer AAnalyte 800) and the solid residual collected by the membrane filter (iron-impregnated solids) was dried in air for 48 hours and stored at 4℃ prior to use. In the case where Fe(II) (sulfate solution) was used as the iron precursor, it follows an identical procedure as Fe(III) adsorption experiments except that the solution pH was controlled at 6 +/- 0.1 with 5 mM MES. Specifically, an aliquot of MES was added to sodium chloride solution before the addition of the Fe(II) stock solution. After dilution to 500 mL, pH of the solution was adjusted by primarily titrating with 10% (v/v) sodium hydroxide to pH = 6. 20% (v/v) hydrochloric acid (HCl) was also used to bring pH up to 6 occasionally when sodium hydroxide was overdosed. The bottle was open to air throughout the adsorption period with the use of a perforated parafilm cover. Solution pH of all experiments was recorded by a Mettler Toledo portable pH meter (SevenGo™ SG2), which was calibrated on a daily basis. The calibration of pH meter was completed by three-point calibration with buffers of pH = 4.01, 7.0 and 10.01.

Table 2.1. Experimental conditions for iron impregnation via simple aqueous adsorption procedure.

| **Soilds** | **Metal precursor* and amount added** | **Resulting concentration of metal ion** | **Background electrolytes** | **Solution volume** | **Mixing method and time** | **pH at the end of adsorption** | **Collecting method** | **Drying method and time** |
|---|---|---|---|---|---|---|---|---|
| 0.3 g Aero$Al_2O_3$ | $FeCl_3$ 1.25 mL | 0.05 mM | 10mM NaCl | 500 mL | shaking at 250 rpm for 24 hours | 4.81 | vacuum filteration | Air dry at 25˚C for ~48 hours |
| 0.3 g Aero$Al_2O_3$ | $FeCl_3$ 2.5 mL | 0.1 mM | 10mM NaCl | 500 mL | shaking at 250 rpm for 24 hours | 4.67 | vacuum filteration | Air dry at 25˚C for ~48 hours |
| 0.3 g Aero$Al_2O_3$ | $FeCl_3$ 5 mL | 0.2 mM | 10mM NaCl | 500 mL | shaking at 250 rpm for 24 hours | 4.35 | vacuum filteration | Air dry at 25˚C for ~48 hours |
| 0.3 g Aero$Al_2O_3$ | $FeCl_3$ 10 mL | 0.4 mM | 10mM NaCl | 500 mL | shaking at 250 rpm for 24 hours | 3.65 | vacuum filteration | Air dry at 25˚C for ~48 hours |
| 0.3 g Aero$Al_2O_3$ | $FeCl_3$ 20 mL | 0.8 mM | 10mM NaCl | 500 mL | shaking at 250 rpm for 24 hours | 2.78 | vacuum filteration | Air dry at 25˚C for ~48 hours |
| 0.3 g Aero$Al_2O_3$ | $FeCl_3$ 40 mL | 1.6 mM | 10mM NaCl | 500 mL | shaking at 250 rpm for 24 hours | n/a | vacuum filteration | Air dry at 25˚C for ~48 hours |
| 0.3 g Aero$Al_2O_3$ | $FeSO_4$ 1 mL | 0.01 mM | 5 mM NaCl, 5 mM MES | 500 mL | shaking at 250 rpm for 24 hours | ~ 6 | vacuum filteration | Air dry at 25˚C for ~48 hours |
| 0.3 g Aero$Al_2O_3$ | $FeSO_4$ 2 mL | 0.02 mM | 5 mM NaCl, 5 mM MES | 500 mL | shaking at 250 rpm for 24 hours | ~ 6 | vacuum filteration | Air dry at 25˚C for ~48 hours |
| 0.3 g Aero$Al_2O_3$ | $FeSO_4$ 5 mL | 0.05 mM | 5 mM NaCl, 5 mM MES | 500 mL | shaking at 250 rpm for 24 hours | 6.20 | vacuum filteration | Air dry at 25˚C for ~48 hours |
| 0.3 g Aero$Al_2O_3$ | $FeSO_4$ 10 mL | 0.1 mM | 5 mM NaCl, 5 mM MES | 500 mL | shaking at 250 rpm for 24 hours | ~ 6 | vacuum filteration | Air dry at 25˚C for ~48 hours |
| 0.3 g Aero$Al_2O_3$ | $FeSO_4$ 20 mL | 0.2 mM | 5 mM NaCl, 5 mM MES | 500 mL | shaking at 250 rpm for 24 hours | ~ 6 | vacuum filteration | Air dry at 25˚C for ~48 hours |
| 0.3 g Aero$Al_2O_3$ | $FeSO_4$ 40 mL | 0.4 mM | 5 mM NaCl, 5 mM MES | 500 mL | shaking at 250 rpm for 24 hours | ~ 6 | vacuum filteration | Air dry at 25˚C for ~48 hours |
| 0.3 g Aero$Al_2O_3$ | $FeSO_4$ 80 mL | 0.8 mM | 5 mM NaCl, 5 mM MES | 500 mL | shaking at 250 rpm for 24 hours | ~ 6 | vacuum filteration | Air dry at 25˚C for ~48 hours |
| 0.3 g Aero$SiO_2$ | $FeCl_3$ 2.5 mL | 0.1 mM | 10mM NaCl | 500 mL | shaking at 250 rpm for 24 hours | 3.47 | vacuum filteration | Air dry at 25˚C for ~48 hours |
| 0.3 g Aero$SiO_2$ | $FeCl_3$ 5 mL | 0.2 mM | 10mM NaCl | 500 mL | shaking at 250 rpm for 24 hours | 2.95 | vacuum filteration | Air dry at 25˚C for ~48 hours |

Table 2.1. Continued

| **Soilds** | **Metal precursor* and amount added** | **Resulting concentration of metal ion** | **Background electrolytes** | **Solution volume** | **Mixing method and time** | **pH at the end of adsorption** | **Collecting method** | **Drying method and time** |
|---|---|---|---|---|---|---|---|---|
| 0.3 g $AeroSiO_2$ | $FeCl_3$ 10 mL | 0.4 mM | 10mM NaCl | 500 mL | shaking at 250 rpm for 24 hours | 2.77 | vacuum filteration | Air dry at 25˚C for ~48 hours |
| 0.3 g $AeroSiO_2$ | $FeCl_3$ 20 mL | 0.8 mM | 10mM NaCl | 500 mL | shaking at 250 rpm for 24 hours | 2.28 | vacuum filteration | Air dry at 25˚C for ~48 hours |
| 0.3 g $AeroSiO_2$ | $FeCl_3$ 40 mL | 1.6 mM | 10mM NaCl | 500 mL | shaking at 250 rpm for 24 hours | 2.00 | vacuum filteration | Air dry at 25˚C for ~48 hours |
| 0.3 g $AeroSiO_2$ | $FeSO_4$ 1 mL | 0.01 mM | 5 mM NaCl, 5 mM MES | 500 mL | shaking at 250 rpm for 24 hours | ~ 6 | vacuum filteration | Air dry at 25˚C for ~48 hours |
| 0.3 g $AeroSiO_2$ | $FeSO_4$ 2 mL | 0.02 mM | 5 mM NaCl, 5 mM MES | 500 mL | shaking at 250 rpm for 24 hours | ~ 6 | vacuum filteration | Air dry at 25˚C for ~48 hours |
| 0.3 g $AeroSiO_2$ | $FeSO_4$ 10 mL | 0.1 mM | 5 mM NaCl, 5 mM MES | 500 mL | shaking at 250 rpm for 24 hours | 5.90 | vacuum filteration | Air dry at 25˚C for ~48 hours |
| 0.3 g $AeroSiO_2$ | $FeSO_4$ 20 mL | 0.2 mM | 5 mM NaCl, 5 mM MES | 500 mL | shaking at 250 rpm for 24 hours | 5.85 | vacuum filteration | Air dry at 25˚C for ~48 hours |
| 0.3 g $AeroSiO_2$ | $FeSO_4$ 40 mL | 0.4 mM | 5 mM NaCl, 5 mM MES | 500 mL | shaking at 250 rpm for 24 hours | 5.77 | vacuum filteration | Air dry at 25˚C for ~48 hours |
| 0.3 g $AeroSiO_2$ | $FeSO_4$ 80 mL | 0.8 mM | 5 mM NaCl, 5 mM MES | 500 mL | shaking at 250 rpm for 24 hours | n/a | vacuum filteration | Air dry at 25˚C for ~48 hours |
| 0.3 g $AeroSiO_2$ | $FeSO_4$ 120 mL | 1.2 mM | 5 mM NaCl, 5 mM MES | 500 mL | shaking at 250 rpm for 24 hours | 5.36 | vacuum filteration | Air dry at 25˚C for ~48 hours |
| 0.3 g $AeroSiO_2$ | $FeSO_4$ 160 mL | 1.6 mM | 5 mM NaCl, 5 mM MES | 500 mL | shaking at 250 rpm for 24 hours | 5.14 | vacuum filteration | Air dry at 25˚C for ~48 hours |

* Stock solution for Ferric precursor was at 20 mM for Fe(III) concentration; stock for Ferrous precursor was at 5 mM Fe(II) concentration.

## 2.4. Measurement of catalytic activity through catalyzed benzoate oxidation

All catalytic reactions were carried out in the dark by wrapping the glass vials with aluminum foil to exclude possible photocatalytic processes. Two aqueous contaminant transformation tests were performed. The probe compound chosen in both tests was benzoate (hereafter referred to as BA) for the reason that benzoate reacts selectively with hydroxyl radicals among other possible oxidants (Baker & Gebicki, 1984). Benzoic acid is a weak acid with a pKa = 4.19 and will dissociate with increasing solution pH (Figure 2.1), therefore benzoic acid ($C_7H_5O_2$-H) and benzoate ($C_7H_5O_2^-$) may coexist within the pH range of this study (from 4.0 to neutral). A potential complicating factor is that BA has a strong adsorptive affinity for the solid substrates used in this study (Cornell & Schwertmann, 2006; Das *et al.*, 2005; GUAN *et al.*, 2007). To correct the total concentration change of BA for its adsorption to the solids, parallel control experiments were carried out to measure the adsorption of BA by Fe-impregnated solids (Table 2.2, experiment 1 and 3-6). 0.03 gram of artificial solids and 0.2 mL of BA stock solution at 10 ppm were added into a 40-mL glass vial in order and the mixture was diluted to 20 mL with DDI. After ultrasonication (~3min) to ensure thorough mixing of solids and the solution, vials were wrapped again with brown paper and loaded on a wrist-action mechanical shaker at a mixing speed of ~250 rpm over the whole test period (24 hours). Initial concentration was obtained by sampling the “control_adsorption” (Table 2.2) of each experiment at 0 hour. Samples were taken at predetermined intervals (4 , 8 and 24 hours, variation of +/- an hour occurred for sampling convenience) and passed through

0.2 μm syringe filters (Millipore SLLG025SS, hydrophilic, PTFE, 25 mm, ethylene oxide sterilized) into amber 2-mL HPLC vials . A small amount (32 μL) of methanol was added to vials before sample was injected in as a radical scavenger to quench any further oxidation (even though there cannot be oxidation in this case but only in the second test explained below, addition of methanol still was carried out to maintain constant experimental background). A thorough mixing manually was also guaranteed right before sampling to ensure the solid to liquid ratio was not affected by sampling. Samples then were analyzed by a Hewlett Packard 1100 series high performance liquid chromatography system (HPLC) equipped with a Grace C18 column within 24 hours of sample collection. The eluent used for BA analysis was acetonitrile and 10 mM HCl solution at a volume ratio of 30:70 and the eluent was mixed well before supplying to HPLC eluent tank. A calibration curve for BA was constructed with peak areas read at 220 nm wavelength. Solution pH of all experiments was recorded by a Mettler Toledo portable pH meter, which was calibrated on a daily basis.

Table 2.2. Example of typical experimental setup for contaminant transformation tests.

| | **Experiment description** | **Benzoate** | **Volume** | **Mass of solid** | **Vial wrapping?** | **Ultrasound** | **$H_2O_2$** | **Sample time 1** | **Sample time 2** | **Sample time 3** | **Sample time 4** | **Sample time 5** | **Sample time 6** |
|---|---|---|---|---|---|---|---|---|---|---|---|---|---|
| 1 | Control-adsorption | 10 mg/L | 20 ml | NA | Y | ~ 3 min | 0 | 0 h | - | 4 h | - | 8 h | 24 h |
| 2 | Control | 10 mg/L | 40 ml | NA | Y | ~ 3 min | 500 ul | 0 h | 2 h | 4 h | 6 h | 8 h | 24 h |
| 3 | 0.1 mM Fe(II)_$SiO_2$_ adsorption | 10 mg/L | 20 ml | 30 mg | Y | ~ 3 min | 0 | | - | 4 h | - | 8 h | 24 h |
| 4 | 0.2 mM Fe(II)_$SiO_2$_ adsorption | 10 mg/L | 20 ml | 30 mg | Y | ~ 3 min | 0 | | - | 4 h | - | 8 h | 24 h |
| 5 | 0.4 mM Fe(II)_$SiO_2$_ adsorption | 10 mg/L | 20 ml | 30 mg | Y | ~ 3 min | 0 | | - | 4 h | - | 8 h | 24 h |
| 6 | 0.8 mM Fe(II)_$SiO_2$_ adsorption | 10 mg/L | 20 ml | 30 mg | Y | ~ 3 min | 0 | | - | 4 h | - | 8 h | 24 h |
| 7 | 0.1 mM Fe(II)_$SiO_2$ | 10 mg/L | 40 ml | 60 mg | Y | ~ 3 min | 500 ul | | 2 h | 4 h | 6 h | 8 h | 24 h |
| 8 | 0.2 mM Fe(II)_$SiO_2$ | 10 mg/L | 40 ml | 60 mg | Y | ~ 3 min | 500 ul | | 2 h | 4 h | 6 h | 8 h | 24 h |
| 9 | 0.4 mM Fe(II)_$SiO_2$ | 10 mg/L | 40 ml | 60 mg | Y | ~ 3 min | 500 ul | | 2 h | 4 h | 6 h | 8 h | 24 h |
| 10 | 0.8 mM Fe(II)_$SiO_2$ | 10 mg/L | 40 ml | 60 mg | Y | ~ 3 min | 500 ul | | 2 h | 4 h | 6 h | 8 h | 24 h |

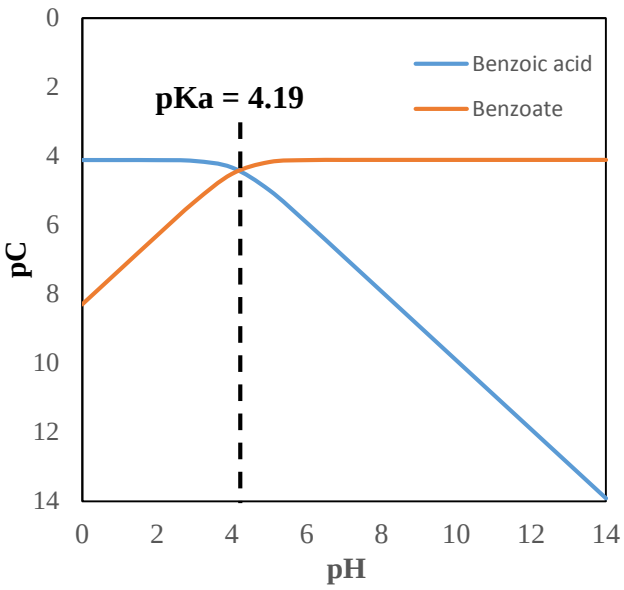


Figure 2.1. pC-pH diagram for aqueous Sodium Benzoate at concentration of 10 mg/L.

The second set of experiments named as BA-degradation were intended to examine the rate of BA oxidation catalyzed by the iron-impregnated solids in the presence of hydrogen peroxide. Similar procedure as that of BA-adsorption experiments was followed, except that 500 µL of 3% (w/w) hydrogen peroxide was added to the solution after ultrasonication (Table 2.2, experiment 2, 7-10). All the vials for the BA-degradation experiments were double wrapped (foil and brown paper) and mixed on a shaker at 250 rpm as well. Sampling the control (Table 2.2, experiment 2) at 0 hour gave the initial Benzoate concentration and sampling for experiment 2, 7-10 afterwards followed identical steps clarified above in the BA-adsorption procedure, yet predetermined sampling intervals increased to 2, 4, 6, 8 and 24 hours (in order to investigate kinetics of catalytic reactions). Final pH of the solution phase was also recorded.

To investigate the pH effect on BA-degradation rates, several Good's buffers including 5 mM MES (pH 5.5), MOPS (pH 7.0) and HEPES (pH 8.2) were used. The experiment solutions were pre-adjusted to desired pHs (expressed in parentheses) before the addition of catalysts and $H_2O_2$. Other conditions and procedures follow those described above.

# Chapter 3

# Results

## 3.1. Aqueous catalytic oxidation of benzoate

Distinct adsorption results were noted for four types of iron-impregnated solid phases. To be specific, the iron-impregnated solid phases differed by their precursors for impregnation (Fe(II) or Fe(III)) and by the concentration of precursor during the aqueous impregnation. The diversity in type of precursor and concentration of precursor gave rise to different quantity of iron impregnated (Table 3.1) and also iron species of different valences. The resulting iron-enriched surfaces demonstrated varied surface properties. pH influenced oxidation rate of benzoate acid to a large extent.

### 3.1.1. Adsorption of benzoate to iron-impregnated solids

Adsorption experiments of benzoate were conducted to evaluate the adsorption capacity of iron-impregnated alumina and silica as illustrated in Figure 3.1. pH adjustment of benzoate solution was performed prior to the addition of iron-impregnated solids, so that initial pH of the adsorption test of a certain impregnated solid was equal to the final pH of its oxidation experiment (Table 3.2). Adsorption completed in less than 4 hours based on results of former tests (not shown), and thus sample for benzoate analysis was obtained at the end of the fourth hour of adsorption.

Solids that were impregnated with Fe(II) precursor (referred to as Fe(II)_alumina, Fe(II)_silica afterwards) showed limited adsorption of benzoate. pH edge studies were conducted for adsorption of benzoate to pristine silica, pristine alumina and nano-sized ferric oxide, and the result is illustrated by Figure 3.2. Adsorption pH edge refers to a pH where the adsorption of a solute changes sharply from about 10% to about 90% of its total adsorbable amount. It was evident that silica adsorbed little benzoate over pH 3-10. The adsorption of benzoate to alumina reached 20% when initial concentration of benzoate was 10 ppm.

Adsorption behaviors of benzoate on Fe(III)_alumina and Fe(III)_silica showed clear influence that iron impregnation had brought to the substrate. In addition to the considerate enhancement on amount of benzoate adsorbed, adsorption capacity of both Fe(III)_silica and Fe(III)_alumina demonstrated a stronger dependence on the quantity of Fe(III) impregnated.

Table 3.1. Amount of Fe atoms adsorbed onto surfaces of nanosized alumina and nanosized silica

| Precursor type | Precursor Concentration | Solid type | Surface loading (mg Fe/$m^2$) | % adsorbed | pH at the end of adsorption | Solid type | Surface loading (mg Fe/$m^2$) | % adsorbed | pH at the end of adsorption |
|---|---|---|---|---|---|---|---|---|---|
| Fe (II) | 0.01 mM | Aero$Al_2O_3$ | n/a | 90% | ~ 6 with 5 mM MES buffering | Aero$SiO_2$ | n/a | 106% | ~ 6 with 5 mM MES buffering |
| | 0.02 mM | Aero$Al_2O_3$ | n/a | 73% | | Aero$SiO_2$ | n/a | 90% | |
| | 0.1 mM | Aero$Al_2O_3$ | 0.044 | 48% | | Aero$SiO_2$ | 0.037 | 79% | |
| | 0.2 mM | Aero$Al_2O_3$ | 0.100 | 54% | | Aero$SiO_2$ | 0.077 | 82% | |
| | 0.4 mM | Aero$Al_2O_3$ | 0.271 | 73% | | Aero$SiO_2$ | 0.153 | 81% | |
| | 0.8 mM | Aero$Al_2O_3$ | 0.556 | 75% | | Aero$SiO_2$ | 0.242 | 64% | |
| | 1.2 mM | - | | | | Aero$SiO_2$ | 0.433 | 77% | |
| | 1.6 mM | - | | | | Aero$SiO_2$ | 0.494 | 66% | |
| Fe (III) | 0.1 mM | Aero$Al_2O_3$ | 0.093 | 100% | 4.67 | Aero$SiO_2$ | 0.044 | 95% | 3.47 |
| | 0.2 mM | Aero$Al_2O_3$ | 0.186 | 100% | 4.35 | Aero$SiO_2$ | 0.084 | 92% | 2.95 |
| | 0.4 mM | Aero$Al_2O_3$ | 0.346 | 96% | 3.65 | Aero$SiO_2$ | 0.150 | 86% | 2.77 |
| | 0.8 mM | Aero$Al_2O_3$ | 0.693 | 92% | 2.78 | Aero$SiO_2$ | 0.238 | 63% | 2.28 |
| | 1.6 mM | Aero$Al_2O_3$ | 1.018 | 72% | n/a | Aero$SiO_2$ | 0.384 | 51% | 2.00 |

Table 3.2. Final pHs for benzoate-adsorption tests, benzoate-oxidation tests and pH edge study.

| Solid identification | Experiment description | Final pH | Experiment description | Final pH | Solid identification | Experiment description | Final pH | Experiment description | Final pH |
|---|---|---|---|---|---|---|---|---|---|
| 0.05 mM Fe(II)_$Al_2O_3$ | | 5.07 | | 4.58 | | | | | |
| 0.1 mM Fe(II)_$Al_2O_3$ | contaminant adsorption | 5.02 | contaminant oxidation | 4.57 | 0.1 mM Fe(II)_$SiO_2$ | | 5.18 | | 4.165 |
| 0.2 mM Fe(II)_$Al_2O_3$ | | 4.93 | | 4.55 | 0.2 mM Fe(II)_$SiO_2$ | | 5.19 | | 4.16 |
| 0.4 mM Fe(II)_$Al_2O_3$ | | 4.60 | | 4.46 | 0.4 mM Fe(II)_$SiO_2$ | contaminant adsorption | 5.12 | contaminant oxidation | 4.17 |
| 0.8 mM Fe(II)_$Al_2O_3$ | | 4.65 | | 4.39 | 0.8 mM Fe(II)_$SiO_2$ | | 5.15 | | 4.025 |
| | | | | | 1.2 mM Fe(II)_$SiO_2$ | | 5.17 | | 3.98 |
| | | | | | 1.6 mM Fe(II)_$SiO_2$ | | 5.16 | | 3.9 |
| 0.05 mM Fe(III)_$Al_2O_3$ | | 4.75 | | 4.47 | | | | | |
| 0.1 mM Fe(III)_$Al_2O_3$ | | 4.98 | | 4.45 | 0.1 mM Fe(III)_$SiO_2$ | | 5.11 | | 4.19 |
| 0.2 mM Fe(III)_$Al_2O_3$ | contaminant adsorption | 4.62 | contaminant oxidation | 4.35 | 0.2 mM Fe(III)_$SiO_2$ | contaminant adsorption | 5.07 | contaminant oxidation | 4.14 |
| 0.4 mM Fe(III)_$Al_2O_3$ | | 3.29 | | 4.19 | 0.4 mM Fe(III)_$SiO_2$ | | 5.11 | | 4.1 |
| 0.8 mM Fe(III)_$Al_2O_3$ | | 4.28 | | 4.17 | 0.8 mM Fe(III)_$SiO_2$ | | 5.03 | | 4.06 |
| 1.6 mM Fe(III)_$Al_2O_3$ | | 4.98 | | 4.07 | 1.6 mM Fe(III)_$SiO_2$ | | 5.1 | | 3.86 |
| pH edge study Aero$Al_2O_3$ | initial pH = 3.00 | 3.33 | | | pH edge study Aero$SiO_2$ | initial pH = 2.95 | 2.98 | | |
| | initial pH = 4.12 | 4.98 | | | | initial pH = 4.09 | 4.1 | | |
| | initial pH = 5.30 | 5.34 | | | | initial pH = 5.10 | 5.02 | | |
| | initial pH = 6.02 | 5.41 | | | | initial pH = 6.00 | 5.62 | | |
| | initial pH = 7.18 | 5.84 | | | | initial pH = 7.02 | 4.64 | | |
| | initial pH = 8.77 | 5.86 | | | | initial pH = 8.40 | 6.82 | | |
| | initial pH = 10.27 | 7.28 | | | | initial pH = 10.25 | 7.32 | | |

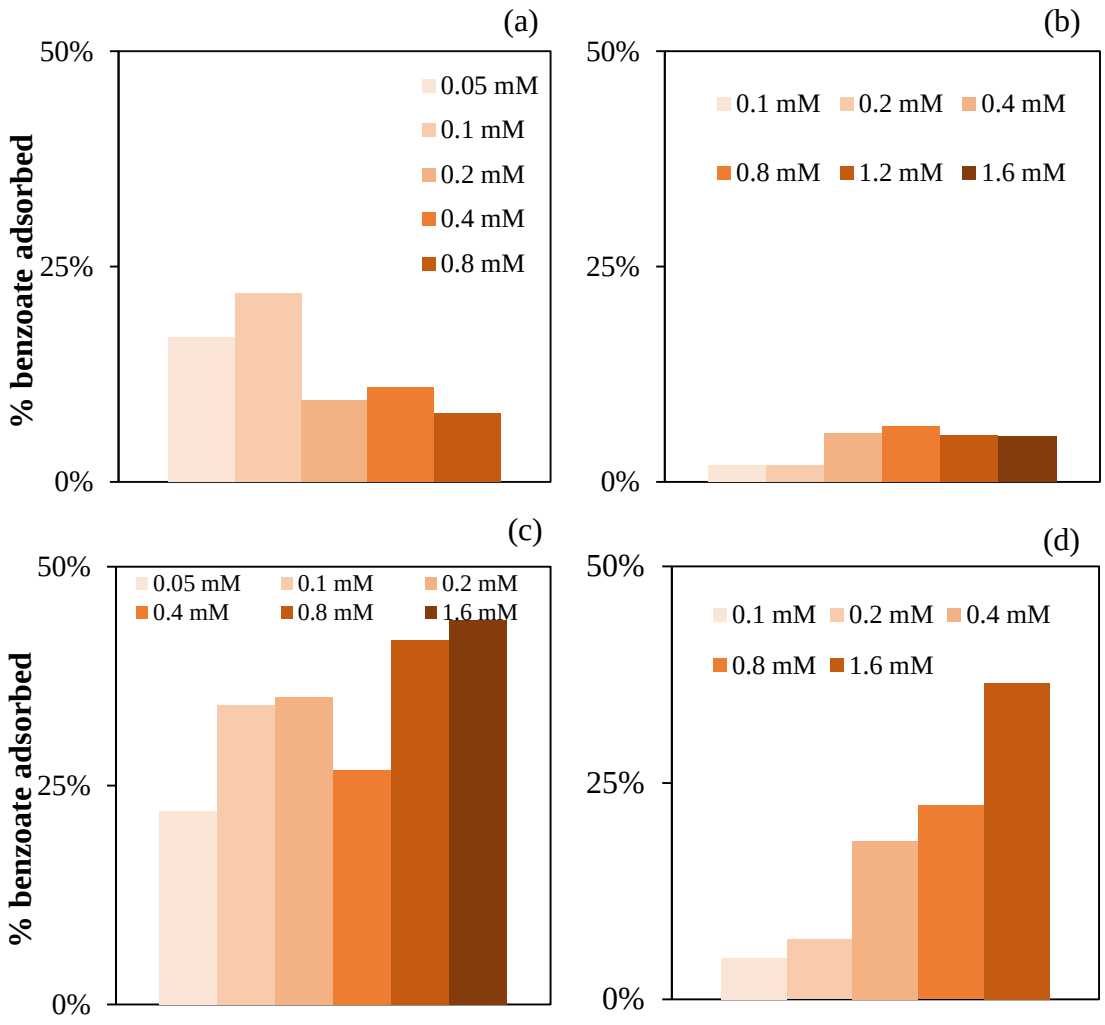


Figure 3.1. Adsorption of benzoate to iron-impregnated silica and alumina particles. a) iron-impregnated alumina, Fe(II) as precursor; b) iron-impregnated silica, Fe(II) as precursor; c) iron-impregnated aluminam Fe(III) as precursor and d) iron-impregnated silica, Fe(III) as precursor.

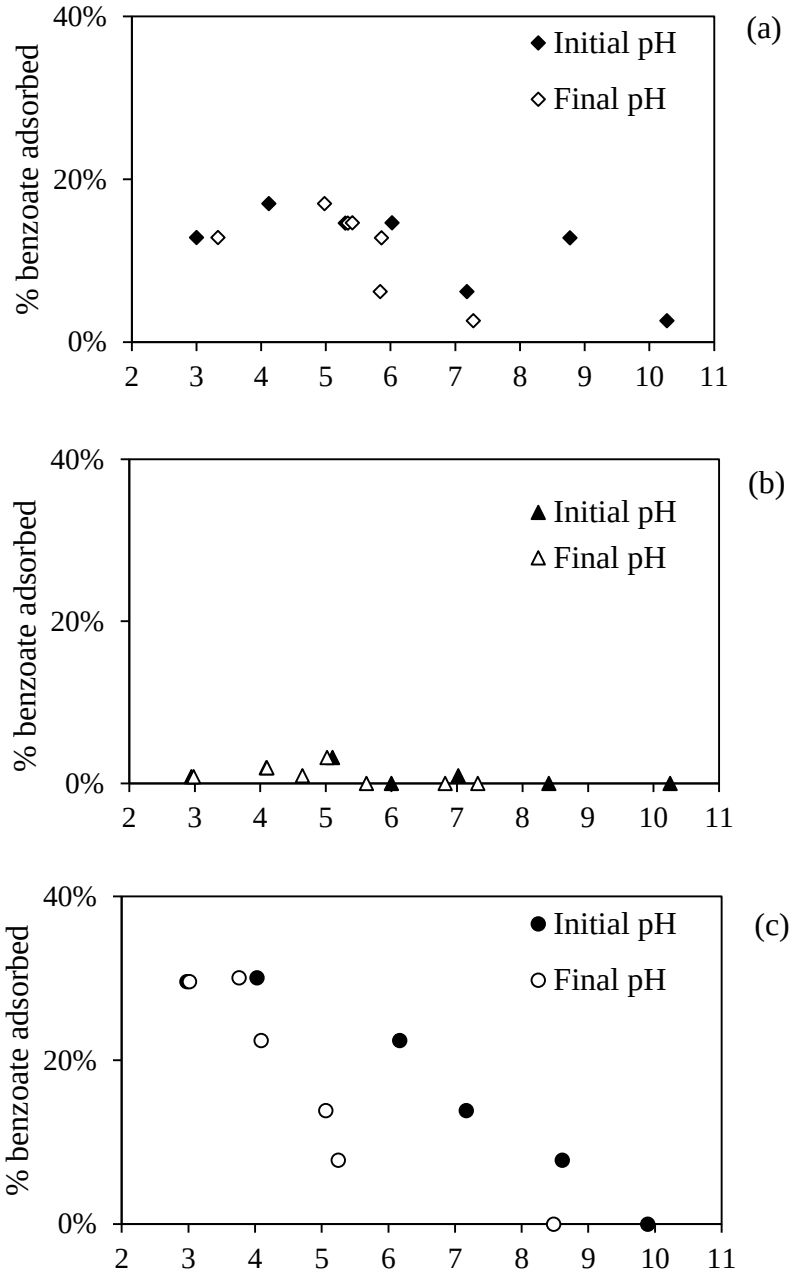


Figure 3.2. pH edge study for adsorption of benzoate on a) aeroalumina, b) aerosilica and c) nanosized ferric oxide. Initial pH was adjusted by titrating the benzoate aqueous solution with hypochloric acid (20%, v/v) or Sodium hydroxide (10%, w/w) before addition of solid phases. No pH buffer was used throughout the adsorption process. Percentages adsorbed were presented with respect to both intial pH and final pH.

### 3.1.2. Catalytic activity of solids exposed to Fe(II) or Fe(III) solutions

The oxidation experiments examined oxidation of benzoate through Fenton processes (Section 1.2.1) catalyzed by iron-impregnated particles. The results certified the catalytic ability of surface iron species and such catalytic ability varied when different substrates was used for impregnation (Figure 3.3). In general, the kinetic rate of benzoate oxidation did not exhibit apparent kinetic order. Even with an excess amount of $H_2O_2$ added, the kinetics did not conform to a pseudo-first-order trend. It is considered that the adsorption and desorption of benzoate took place not only simultaneously but interactively with catalytic oxidation of benzoate, and therefore no evident reaction order was revealed. To examine the extent of benzoate oxidation, it was necessary to discount surface adsorption of benzoate. Assuming that adsorption attained equilibrium in less than 2 hours, the average oxidation rate of benzoate can be approximated from its concentration change in 2 - 8 hour experimental period (in some case, 2 – 6 hour). Specifically the amount of benzoate eliminated in 2 – 8 hour experimental period was presented in the unit of mole by multiplying the difference of remaining percentage at 2 hours and that at 8 hours by initial amount of benzoate in unit of mole. Average oxidation rate was then calculated (refer to eq 3.1). Average oxidation rate of benzoate obtained were then plotted against the surface density of Fe atom as in Figure 3.4. Surface density was calculated by dividing the measured quantity of Fe impregnated by the BET surface area of the substrates (refer to eq 3.2). Since benzoate can solely be oxidized by ·OH (Baker & Gebicki, 1984), the decrease of benzoate should be interpreted as the generation of

hydroxyl radical, instead of the mineralization of aromatic acid (ultimate breakdown to carbon dioxide).

$$Average\ oxidation\ rate = \frac{\left(\frac{Concentration\ of\ benzoate\ at\ t_1}{initial\ concentration\ of\ benzoate} - \frac{Concentration\ of\ benzoate\ at\ t_2}{initial\ concentration\ of\ benzoate}\right) \times initial\ moles\ of\ benzoate}{t_1 - t_2} \quad (3.1)$$

$$Surface\ density = \frac{moles\ of\ Fe\ adsorbed \times (6.02 \times 10^{23})}{BET\ surface\ area\ of\ pristine\ solid\ phase} \quad (3.2)$$

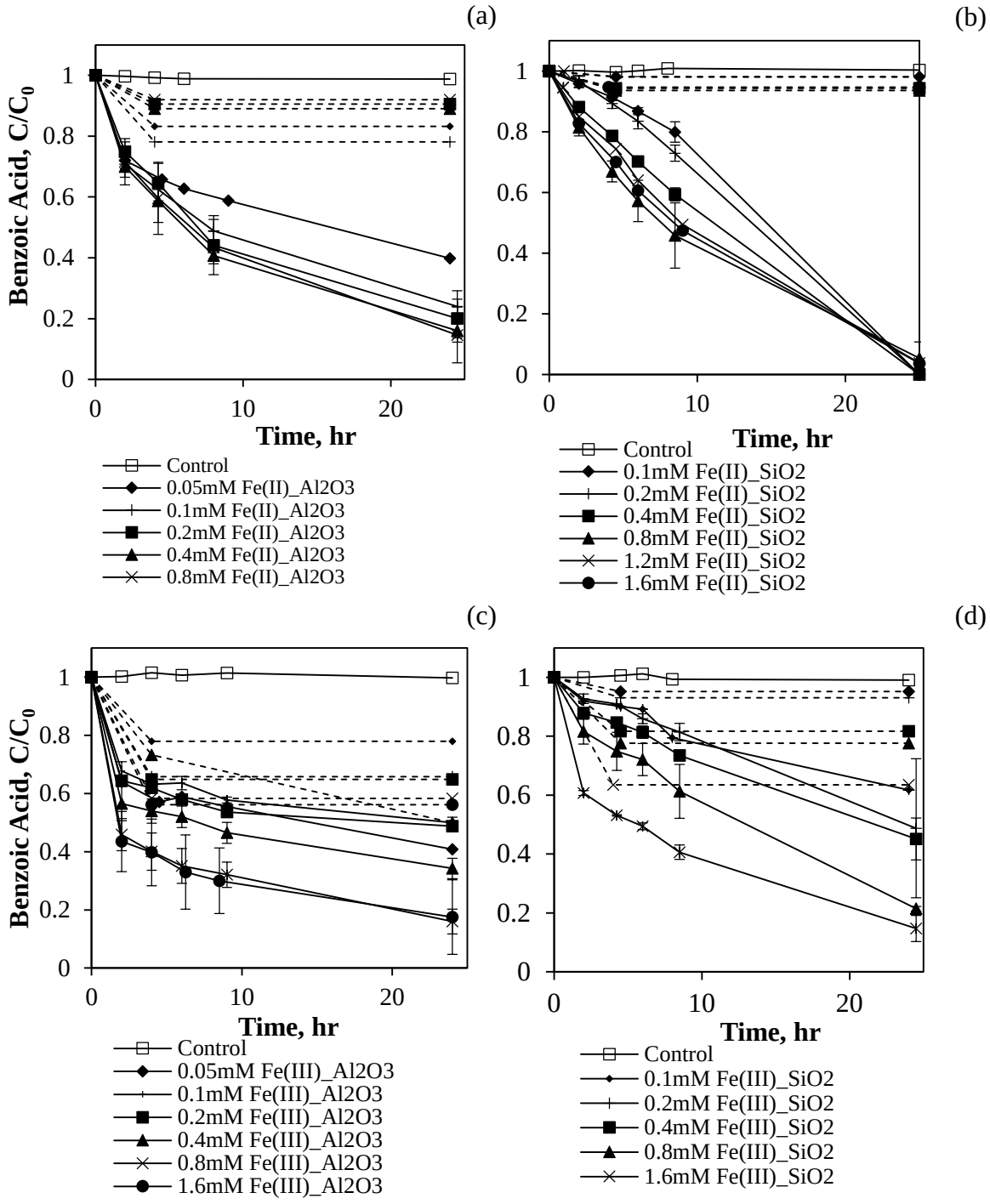


Figure 3.3. Transformation of benzoate catalyzed by iron-impregnated solids in the presence of hydrogen peroxide. a) iron-impregnated alumina, Fe(II) as precursor; b) iron-impregnated silica, Fe(II) as precursor; c) iron-impregnated aluminam Fe(III) as precursor and d) iron-impregnated silica, Fe(III) as precursor. Dashed lines signify the adsorption of benzoate obtained by the impregnated solid phases.

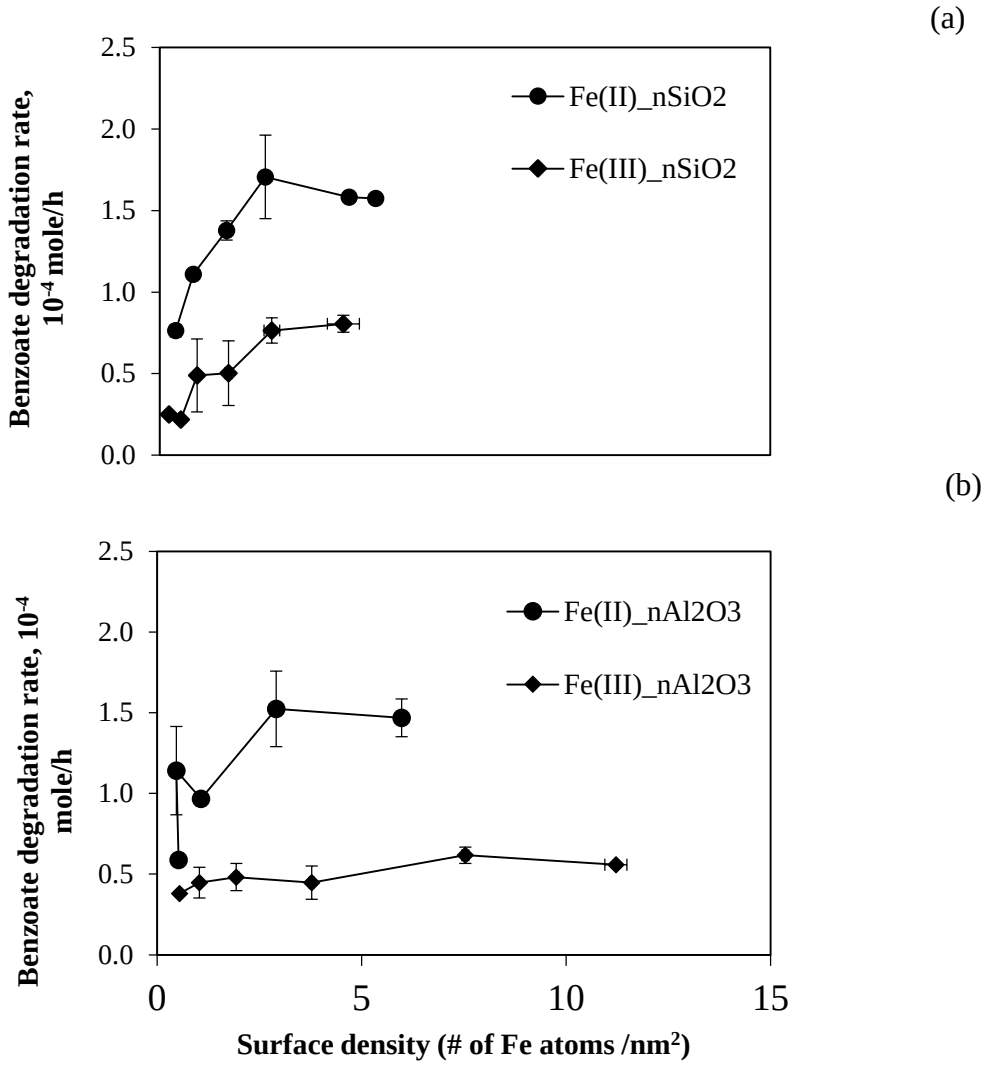


Figure 3.4. Oxidative transformation rate of benzoate versus surface density of iron impregnation. a) iron-impregnated nanosized silica with Fe(II)/Fe(III) as precursor; b) iron-impregnated nanosized alumina with Fe(II)/Fe(III) as precursor.

Note that in Figure 3.4, catalytic capacities of both Fe(II)_alumina and Fe(II)_silica reach a plateau even with increasing amount of Fe impregnated, and this demonstrated saturation of iron impregnation on both surfaces.

The effect of pH on the reactivity was also assessed by buffering the ambient pH in each batch test at constant value. Three ambient pHs controlled by organic buffers (named in parentheses) were selected for Fe(III)-impregnated solids : 5.5 (MES), 7.0 (MOPS), 8.2 (HEPES). For solid phases prepared with Fe(II) as the precursor, pH 6 (controlled by MES) was chosen as a pH of interest. pH was observed to drop approximate 0.2 unit in all cases immediately after adding impregnated solids and another 0.2 unit after adding $H_2O_2$. Hydroxyl radical can react with benzoate within a broad pH range of 3-11 according to the study of Baker and Gebicki (1984), thus the significant decreases in benzoate oxidation rates occurred in neutral or alkali aqueous environment are due to the decreasing ability of the surfaces to catalyze generation of hydroxyl radical at neutral to alkaline pH.

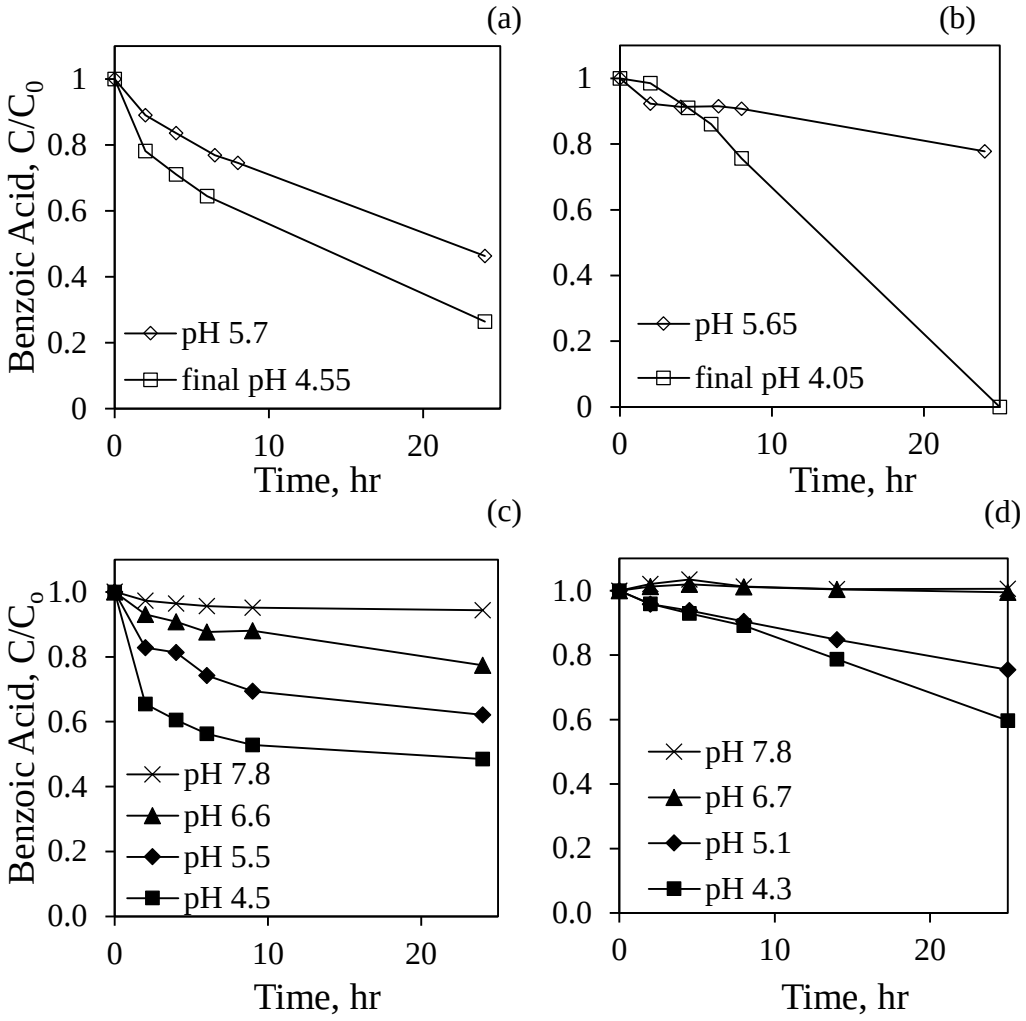


Figure 3.5. Effects of pH on oxidative transformation of benzoate. a) iron-impregnated alumina, Fe(II) as precursor; b) iron-impregnated silica, Fe(II) as precursor; c) iron-impregnated aluminam Fe(III) as precursor and d) iron-impregnated silica, Fe(III) as precursor. [Iron precursor] = 0.2 mM. Average pHs of initial and final pHs (in some cases, final pH) were illustrated in the legends.

## 3.2. Role of nanosized silica and alumina on structure of impregnation

Diffuse reflectance (DR) spectra in the ultraviolent and visible regions were obtained and converted to F(R) spectra as described in Section 2.4 (Figure 3.6). Note that pristine silica

and alumina were used as the reference materials, and because the DR of reference material is deducted from that of the sample, so the bands shown in spectra are caused by iron oxides impregnated on the surface. As is acknowledged, for quantitative analysis through transmission measurements, Beer-Lambert's law (relate the solute's absorption to its concentration in solution) is only valid for diluted samples. Kubelka-Munk function can be used to quantitatively measure the solute of interest "in much the same way" as Beer-Lambert's law, therefore it is not a convincing function to be applied to quantitative analyze condensed samples. Due to the complexity we went through when trying to dilute the original sample and maintain a constant dilution for all the samples, samples as collected after impregnated were analyzed directly without any dilutions. As a result, F(R) spectra obtained by Kubelka-Munk function cannot be interpreted quantitatively. However, by recognizing the significant bands in the spectra and relate those to the DR feature of known structure, it is still possible to qualitatively define the presence of certain structure of iron impregnation. Different structures of surface iron-oxide formation can be revealed and is discussed in Section 4.3.

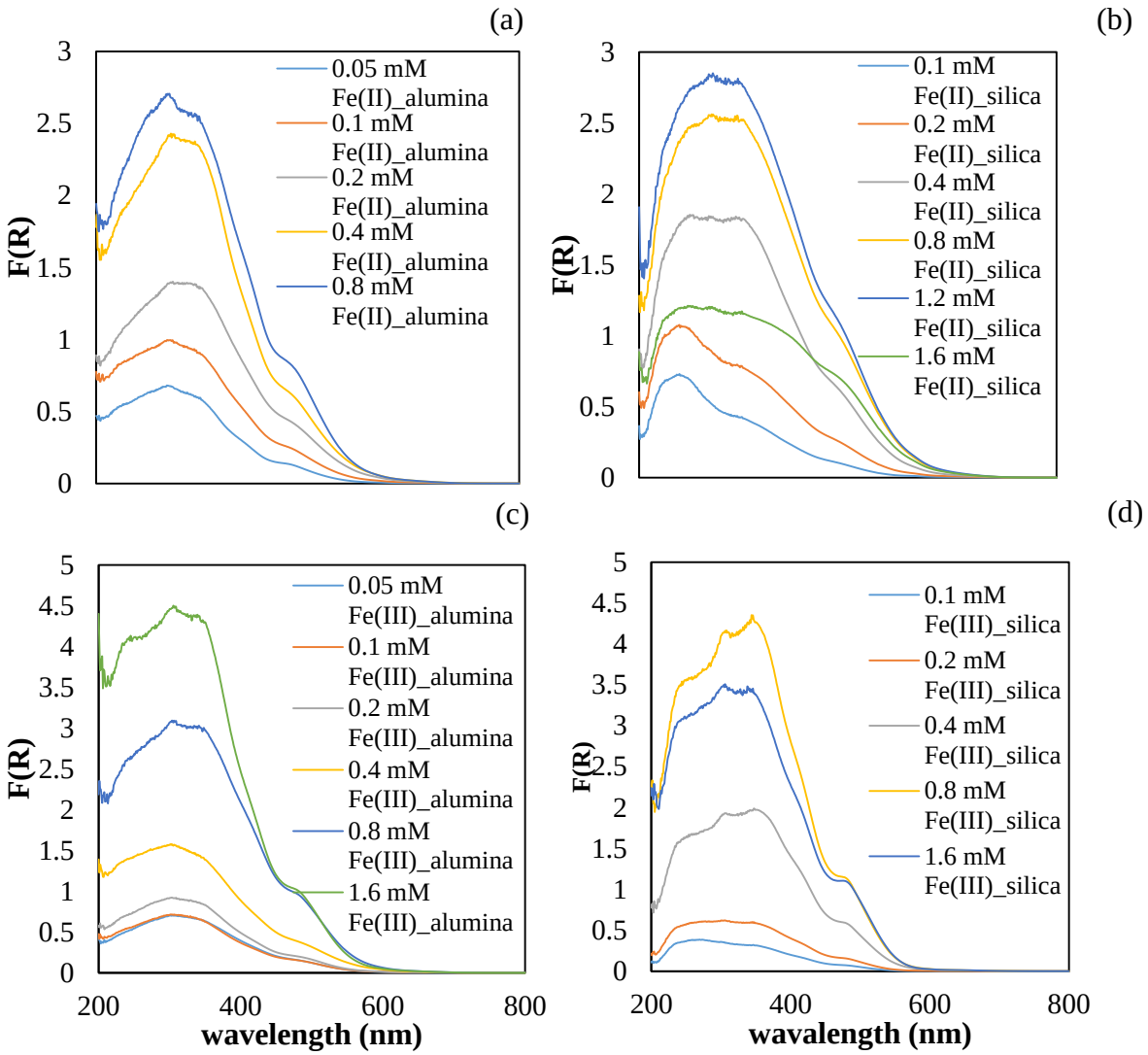


Figure 3.6. DR spectroscopic measurements in the ultraviolent and visible regions of various iron-impregnated solids. a) calculated F(R) at 200-800 nm wavelength for Fe(II) impregnated nanosized $Al_2O_3$; b) Fe(II) impregnated nanosized $SiO_2$; c) Fe(III) impregnated nanosized Al2O3; d) Fe(III) impregnated nanosized $SiO_2$.

# Chapter 4

# Discussion

## 4.1. Interactive impregnation of iron on nanosized alumina

### 4.1.1. Effects of iron impregnation on adsorption capacity of nanosized alumina

A considerable number of studies have investigated the adsorption of benzoate on alumina, proposing both monodentate and irreversible formation of bridged surface complexes under acidic and neutral pH (GUAN *et al.*, 2007; Meier *et al.*, 2009). pH edge study for adsorption of benzoate to pristine alumina revealed that approximately 20% of benzoate was adsorbed to alumina at the current experimental pH (~5) (Figure 3.2). Since no significant increase of benzoate adsorption was noticed when Fe(II)_alumina was tested for adsorption capacity, we can conclude that the impregnation of ferrous iron has limited effects on surface adsorption capacity of alumina. On the contrary, Fe(III) impregnated alumina is shown to enhance the adsorption of benzoate. It is also noticed that an increased quantity of Fe(III) impregnation led to a greater amount of benzoate being adsorbed. Taking into account of the different amounts of benzoate adsorbed to Fe(II)_alumina and that to Fe(III)_alumina, one can infer that impregnation with Fe(III) precursor produces an iron-impregnated surface that can act as a good sorbent.

4.1.2. Catalytic ability of iron impregnated nanosized alumina

It was concluded that the loss of benzoate was chiefly due to oxidation by hydroxyl radicals generated through the catalytic decomposition of $H_2O_2$ on Fe(II)_alumina (Figure 3.3, a), since the surface impregnated with Fe(II) species had limited adsorption capacity. In order to confirm that the oxidation was a heterogeneous transformation, a separate test was performed. The impregnated solids were removed from the solution after 4 hours of reaction by filtering the solution with a syringe filter of 0.2 μm, and the filtrate was allowed to continue to react. No significant decrease in benzoate concentration was observed after the impregnated solids were removed from the solution, signifying that the surface-bound iron species played a major role in the generation of hydroxyl radicals through Fenton-like reaction. This means that oxidative radicals were generated through a heterogeneous process. Specifically, the activation of $H_2O_2$ was assisted by the surface Fe atoms (≡Fe(II) and ≡Fe(III)) and the commonly agreed mechanism was firstly proposed by Haber and Weiss (1934) as illustrated in Scheme 4.1.

Scheme 4.1. Surface catalyzed Fenton reactions

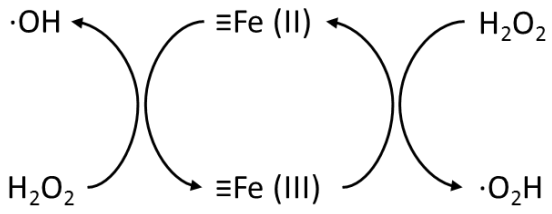


For surfaces loaded with Fe(III) precursors, both the substrate (alumina) and the impregnated iron species interacted with benzoate, which complicated the interpretation

of the result. Adsorption of benzoate to the impregnated solids accounted for the majority of benzoate removal, and the adsorption processes is consistent with the initial rapid decrease of benzoate concentrations in the kinetic data shown in Figure 3.3, c. Thus, the calculated benzoate degradation rates through oxidation, according to the method in Section 3.1.2, eq 3.1, were low when Fe(III)_alumina solids were used (Figure 3.4). Moreover, the rates of oxidative transformation of benzoate by ·OH stay constant, even though more Fe was impregnated on the surface (Figure 3.4). From the catalytic activity of Fe(II)_alumina and Fe(III)_alumina, we can deduce that, when impregnation began with ferrous precursor, the surface of alumina forms interfacial iron species that favor generation of hydroxyl radicals, whereas the iron species formed when ferric precursor was used has significantly lower activity for $H_2O_2$ activation.

Taking into account the results of pH-dependent experiments, we can assess the catalytic activity of the surfaces again. Pham *et al.* (2009) observed lower benzoic acid oxidation rates with increasing pH and they attributed it to the suppression of oxidant generation at higher pH. Although less benzoic acid oxidation occurred, there was more loss of $H_2O_2$ in the pH-controlled experiments than the experiments with no pH control, thus the interference of selected organic buffer, in terms of hydroxyl radical consumption, cannot be excluded. It is noteworthy that, at higher pH, $H_2O_2$ may form “surface-trapped” ·OHs that would be hard for benzoate to access, or it may oxidize iron to hypervalent iron species instead of releasing as free radicals (Scheme 1.1), or it may also quickly decompose to molecular oxygen and water. Additionally, note that the solubility of Fe(III) species is very low in neutral and alkali pH. For even though activation of $H_2O_2$ is

believed to occur on the surface in this case, there might be an equilibrium between the surface iron and soluble Fe required so that cyclic reactions can proceed.

Overall it can be concluded that exposing nanosized alumina to Fe(II)-containing solutions leads to surface with considerable activity for the production of hydroxyl radicals through surface-catalyzed activation of $H_2O_2$, as a result of, relatively high rates of oxidation were observed. On the other hand, exposing to Fe(III) solutions gives rise to a surface deposition of hydrous-ferric-oxide-type formation that offers a significant number of adsorption sites but has lower catalytic ability for $H_2O_2$ activation.

## 4.2. Interactive impregnation of iron on nanosized silica

### 4.2.1. Effects of iron impregnation on adsorption capacity of nanosized silica

There are limited studies reporting the adsorption of benzoate to $SiO_2$, yet it has been suggested that the sorption of benzoate to soil was controlled mainly by the aluminum and iron content but not silica in the soil (Stolpe *et al.*, 1993). The surfaces impregnated with ferrous precursor have little adsorption capacity for benzoate despite the considerate amounts of iron impregnated on the surface as shown in Figure 3.3, b. Likely the electrostatic repulsion resulted between benzoate and the similarly charged nanosized silica caused little adsorption, considering the point of zero charge of silica is typically lower than 4 (Kosmulski, 2009), and within this pH range benzoate is in a neutral (that is to say, undissociated) form as benzoic acid. The anchored Fe atom did not significantly change the electrostatic property of silica.

The impregnation of iron initiated by Fe(III) altered surface of silica for adsorption of benzoate. Appreciable dependence of adsorption capacity on surface density of impregnation is noticed, and this infers that more structure which acted as an adsorbent was formed with more iron impregnation. Notice that only after the concentration of ferrous precursor was greater than 0.2 mM did significant adsorption start to show, meaning that available surface Fe complexes or surface hydroxyl groups for adsorbing benzoate were only formed at higher Fe loadings. As mentioned in earlier content (Section 1.2.2.3), Hu *et al.* (2013) reported that a growth of bulk Fe precipitates are promoted on silica surface by electrostatic forces and structural mismatch. In conjunction with the current adsorption results, when more precipitates grow on surface of silica with increasing impregnation of ferric precursors, they led to increased adsorption of benzoate, we therefore postulate that, only when structure of iron impregnation reached a certain physical size, the impregnated iron become an effective adsorbent for benzoate. However this point should be investigated more thoroughly in future studies.

### 4.2.2. Catalytic ability of iron impregnated nanosized silica

Substantial catalytic ability for Fenton reaction is observed when iron impregnated solids initiated by ferrous precursor was used in benzoate oxidation, and the contaminant transformation was only achieved by oxidation because benzoate adsorbed poorly onto both Fe(II)_silica and pristine silica. As mentioned in Section 4.1.2., a set of experiments was done to confirm the heterogeneity of this oxidative transformation by removing the impregnated silica from the solution after 4 hours of reactions and resuming the aqueous reaction homogeneously for another 20 hours. No more oxidation of benzoate was

detected after impregnated silica was filtered out. Thus, it is concluded that oxidation of benzoate by Fe(II) impregnated silica is mainly through surface iron species heterogeneously. As limited information on the efficiency of various forms of ≡Fe (surface iron species) in activating $H_2O_2$ can be found in the literature, and there is no simple means to characterize the molecular structure of Fe on the surfaces, hence it is hard to determine the chemical basis of the catalytic ability exhibited by the surface iron on both substrates. Nevertheless the hydroxylation and further oxidative transformation of benzoate by ·OH is supposed to occur in the aqueous solution in vicinity to the surface instead of on the surface since the benzoate could not adsorb to surface due to the repulsive force.

Oxidative rate for benzoate experiences a slight increase with more iron impregnation on the surface of silica when Fe(III) was used as the precursor. But the overall catalytic ability of Fe(II)_silica still outperform that of Fe(III)_silica (Figure 3.4). Additionally, one can expect a complete transformation of benzoate within 24 hours when Fe(II)_silica was the catalyst but not in the situation with Fe(III)_silica. This result of benzoate oxidation again proved that different structure of impregnation occurred on surface when different precursors were used as concluded before, to be precise, the structure of iron impregnation formed when ferrous precursor was used possesses good catalytic acitivity for the Fenton reaction, whereas the structure arising from impregnation of ferric precursor has a good benzoate-adsorption capability. In addition, the surface charge of the resulting impregnated silica from ferrous precursor may be different from that of Fe(III)_impregnated silica, given the configuration of iron impregnation is proven to be

controlled by valence of precursor. Whether surface charge is important for surface catalytic reactions requires further systematic investigations.

The significant pH effect on benzoate oxidation that was catalyzed by iron impregnated silica as illustrated in Figures 3.5, b and d can offer some interpretation on surface charge of the impregnated silica. Since the point of zero charge of most silica is less than 4 (Kosmulski, 2009), the surface charge of silica would become more and more negative as the aqueous solution become more alkaline. Plus, benzoate becomes the predominant species in solution as pH increases above 4. Thus, presumably impregnation of iron did not essentially modify surface charge of silica, benzoate received more repulsive forces from the silica surface and consequently failed to approach those surface generated hydroxyl radicals to be oxidized.

## 4.3. Heterogeneous impregnation of iron influenced by substrates and its catalytic ability

The influences that a substrate can have on heterogeneous precipitating of aqueous iron can be further illustrated by UV-Vis spectra (Figure 3.6). It is proposed by Schwidder *et al.* (2005) the bands at around 220 nm and 285 nm are attributable to the electronic transition between oxygen and isolated Fe(III) ions; while bands at 350 nm are demonstration of Fe(III) oligomers; and sub-bands (shoulders) higher than 400 nm reflect large ferric hydroxide particles, that is to say, discrete precipitates.

The spectra of iron-impregnated silica demonstrated a band at ~285 nm which is larger than bands at other wavelengths when low concentration of ferrous precursor (0.1 mM, 0.2 mM) was used for impregnation, which is illustrated in Figure 3.6, b, and this spectral feature signifies the predominant presence of iron as mononuclear adsorbates on the silica surface. At higher concentrations of ferrous precursor, band at 285 nm was no longer obvious, on the other hand, bands at 350 nm and shoulders at high wavelengths (>400 nm) become prevailing. This shift of main bands indicated that when more iron atoms were impregnated on surface of silica, iron oligomers and big precipitates are the primary structure on silica. On the contrary, when ferric precursor was used, the impregnation of iron on silica was promoted to be oligomers even at low loading of ferric iron during impregnation (refer to Figure 3.6, d). Additionally, it is evident that more loading of ferric precursor gave rise to more formation of oligomers and big precipitate.

Bands at ~350 nm and sub-bands at higher than 400 nm constantly stood out in the DR spectra of impregnated alumina, indicating that Fe(III) oligomers and surface precipitation were preferred by surface of alumina regardless of the valence of the iron precursors. One notable observation is that oligomeric clusters are preferred over isolated Fe ions by alumina when low concentration of ferrous precursor was adopted. Still, when there is a higher concentration of Fe ions during impregnation, large particles started to dominate on the surface.

A more direct surface structure was revealed by DR spectra in the ultraviolent and visible regions, and we can relate the uncovered structure to the catalytic ability it brought to the substrate. Specifically, the dominant presence of dispersed iron species (as mononuclear

surface adsorbates) in Fe(II)-initiated impregnation was found on silica, and this adsorbates gave rise to catalytic ability but no adsorption capacity; while Fe(III) oligomers were the primary structure on alumina after Fe(II)-initiated impregnation, and these oligomers also contribute to surface catalysis of Fenton reactions (Figure 3.5, a and b). Moreover, for both substrates, when the concentration of ferrous precursor was high and surface began to show growth of big precipitates, saturation effects on catalytic ability were observed for both surfaces, indicating that precipitates on surface are not good catalysts for $H_2O_2$ activation. In addition to the statement above, the fact that the substrates exposed to aqueous Fe(II) exhibit a higher reactivity in catalyzing Fenton-like reactions while substrates exposed to Fe(III) ions tend to perform as good adsorbent, further confirm that impregnation of isolated Fe and oligomers has good catalytic ability and surface iron precipitates have good adsorption capacity.

# Chapter 5

# Conclusions

The structure and speciation of iron impregnated on solid phases differ significantly when different precursors (Fe(II) or Fe(III)) are used. When ferrous iron is used as the precursor, final structure of the impregnation has a considerable activity to catalyze $H_2O_2$ activation and Fenton-like reactions. The structure, characterized by DR spectra, suggests a dominant formation of iron as mononuclear oligomeric adsorbates. This statement is further bolstered by a saturation effect of benzoate degradation rates with increasing iron loading on the surface, and this is a consequence of large precipitates being formed at higher surface loading, which are not much less catalytically active than the isolated or oligomeric adsorbates. On the contrary, impregnation started with ferric precursor promotes formation of oligomers and precipitates, and this resulting structure demonstrated good benzoate-adsorption properties.

This study shows that mineral substrates have a substantial effect on impregnation of interfacial iron species. For low loading of ferrous iron during impregnation, mononuclear adsorbates are promoted by silica surface while oligomers instead are encouraged on the surface of alumina. Large precipitates grows when increasing loading of iron atoms on both substrates

Benzoate complicates the interpretation of experiment results due to its capacity to adsorb to the substrate and impregnation through multiple mechanism including monodentate complexation, outer-sphere complexation, so future research on the behavior of surface impregnation relies on a better probe compound that interacts with interfacial iron species more selectively. For example, As(III)/As(V) may be a potential adsorbate onto iron-impregnated surfaces, not only because they form an inner-sphere complex with interfacial iron, but arsenite can also be oxidized to arsenate without the presence of oxidants yet only requiring adjacent iron. On this note, it is concluded that interfacial iron species is an interesting group of iron, that is worthy of fundamental investigation so that the environmental significance can be fully understood and eventually be applied to practices of environmental cleanup.

# References

Baker, M. S., & Gebicki, J. M. (1984). The effect of pH on the conversion of superoxide to hydroxyl free radicals. *Archives of biochemistry and biophysics*, *234*(1), 258-264.

Barreiro, J. C., Capelato, M. D., Martin-Neto, L., & Bruun Hansen, H. C. (2007). Oxidative decomposition of atrazine by a fenton-like reaction in a H2O2/ferrihydrite system. *Water Research*, *41*(1), 55-62. doi: http://dx.doi.org/10.1016/j.watres.2006.09.016

Cornell, R. M., & Schwertmann, U. (2006). *The iron oxides: structure, properties, reactions, occurrences and uses*: New York, John Wiley & Sons.

Das, M. R., Bordoloi, D., Borthakur, P. C., & Mahiuddin, S. (2005). Kinetics and adsorption of benzoate and salicylate at the natural hematite–water interface. *Colloids and Surfaces A: Physicochemical and Engineering Aspects*, *254*(1), 49-55.

González-Bahamón, L. F., Hoyos, D. F., Benítez, N., & Pulgarín, C. (2011). New Fe-immobilized natural bentonite plate used as photo-fenton catalyst for organic pollutant degradation. *Chemosphere*, *82*(8), 1185-1189.

González-Bahamón, L. F., Mazille, F., Benítez, L. N., & Pulgarín, C. (2011). Photo-Fenton degradation of resorcinol mediated by catalysts based on iron species supported on polymers. *Journal of Photochemistry and Photobiology A: Chemistry*, *217*(1), 201-206.

Guan, X.-h., Chen, G.-h., & Shang, C. (2007). ATR-FTIR and XPS study on the structure of complexes formed upon the adsorption of simple organic acids on aluminum hydroxide. *Journal of Environmental Sciences*, *19*(4), 438-443.

Gupta, V., Saini, V., & Jain, N. (2005). Adsorption of As (III) from aqueous solutions by iron oxide-coated sand. *Journal of Colloid and Interface Science*, *288*(1), 55-60.

Haber, F., & Weiss, J. (1934). The catalytic decomposition of hydrogen peroxide by iron salts. *Proceedings of the Royal Society of London. Series A, Mathematical and Physical Sciences*, *147*(861), 332-351.

Hanna, K., Kone, T., & Medjahdi, G. (2008). Synthesis of the mixed oxides of iron and quartz and their catalytic activities for the fenton-like oxidation. *Catalysis Communications*, *9*(5), 955-959.

Hu, Y., Neil, C., Lee, B., & Jun, Y. S. (2013, Aug 20). Control of heterogeneous Fe(III) (hydr)oxide nucleation and growth by interfacial energies and local saturations. *Environ Sci Technol,* (47, 16).

Joshi, A., & Chaudhuri, M. (1996). Removal of arsenic from ground water by iron oxide-coated sand. *Journal of environmental engineering, 122*(8), 769-771.

Jun, Y.-S., Lee, B., & Waychunas, G. A. (2010). In situ observations of nanoparticle early development kinetics at mineral− water interfaces. *Environmental science & technology, 44*(21), 8182-8189.

Kosmulski, M. (2009). pH-dependent surface charging and points of zero charge. iv. Update and new approach. *Journal of Colloid and Interface Science, 337*(2), 439-448.

Kwan, W. P., & Voelker, B. M. (2003). Rates of hydroxyl radical generation and organic compound oxidation in mineral-catalyzed Fenton-like systems. *Environmental science & technology, 37*(6), 1150-1158.

Lal, M., Rao, R., Fang, X., Schuchmann, H.-P., & von Sonntag, C. (1997). Radical-induced oxidation of dithiothreitol in acidic oxygenated aqueous solution: a chain reaction. *Journal of the American Chemical Society, 119*(24), 5735-5739.

Larese-Casanova, P., Cwiertny, D. M., & Scherer, M. M. (2010). Nanogoethite formation from oxidation of Fe (II) sorbed on aluminum oxide: implications for contaminant reduction. *Environmental science & technology, 44*(10), 3765-3771.

Larese-Casanova, P., Kappler, A., & Haderlein, S. B. (2012). Heterogeneous oxidation of Fe(II) on iron oxides in aqueous systems: identification and controls of Fe(III) product formation. *Geochimica et Cosmochimica Acta, 91*(0), 171-186. doi: http://dx.doi.org/10.1016/j.gca.2012.05.031

Liou, M.-J., & Lu, M.-C. (2008). Catalytic degradation of explosives with goethite and hydrogen peroxide. *Journal of Hazardous Materials, 151*(2), 540-546.

Lund, C. R., & Dumesic, J. (1981). Strong oxide-oxide interactions in silica-supported magnetite catalysts. 1. X-ray diffraction and Mössbauer spectroscopy evidence for interaction. *The Journal of Physical Chemistry, 85*(21), 3175-3180.

Martinez, F., Calleja, G., Melero, J., & Molina, R. (2007). Iron species incorporated over different silica supports for the heterogeneous photo-fenton oxidation of phenol. *Applied Catalysis B: Environmental, 70*(1), 452-460.

Matta, R., Hanna, K., & Chiron, S. (2007). Fenton-like oxidation of 2,4,6-trinitrotoluene using different iron minerals. *Science of the total environment, 385*(1–3), 242-251. doi: http://dx.doi.org/10.1016/j.scitotenv.2007.06.030

Meier, D. M., Urakawa, A., & Baiker, A. (2009). Adsorption behavior of salicylic, benzoic, and 2-methyl-2-hexenoic acid on alumina: an in situ modulation excitation PM-IRRAS study. *Physical Chemistry Chemical Physics, 11*(43), 10132-10139.

Meng, X., & Korfiatis, G. P. (2001). Removal of arsenic from Bangladesh well water using a household filtration system. *Technologies for Arsenic Removal from Drinking Water. Bangaldesh University of Engineering & Technology (BUET) and United Nation University (UNU)*, 121-130.

Pham, A. L.-T., Lee, C., Doyle, F. M., & Sedlak, D. L. (2009). A silica-supported iron oxide catalyst capable of activating hydrogen peroxide at neutral pH values. *Environmental science & technology, 43*(23), 8930-8935.

Pignatello, J. J., Oliveros, E., & MacKay, A. (2006). Advanced oxidation processes for organic contaminant destruction based on the fenton reaction and related chemistry. *Critical reviews in environmental science and technology, 36*(1), 1-84.

Poulton, S. W., Krom, M. D., & Raiswell, R. (2004). A revised scheme for the reactivity of iron (oxyhydr)oxide minerals towards dissolved sulfide. *Geochimica et Cosmochimica Acta, 68*(18), 3703-3715. doi: http://dx.doi.org/10.1016/j.gca.2004.03.012

Prakash, A., McCormick, A. V., & Zachariah, M. R. (2004). Aero-sol-gel synthesis of nanoporous iron-oxide particles: a potential oxidizer for nanoenergetic materials. *Chemistry of materials, 16*(8), 1466-1471.

Ryan, J. N., & Gschwend, P. M. (1994). Effect of solution chemistry on clay colloid release from an iron oxide-coated aquifer sand. *Environmental science & technology, 28*(9), 1717-1726.

Schwidder, M., Kumar, M. S., Klementiev, K., Pohl, M. M., Brückner, A., & Grünert, W. (2005). Selective reduction of NO with Fe-ZSM-5 catalysts of low Fe content: I. Relations between active site structure and catalytic performance. *Journal of Catalysis, 231*(2), 314-330.

Singer, P. C., & Stumm, W. (1970). Oxygenation of ferrous iron. *Water Poll. Cont. Res. Ser*, 14010-06169.

Snoeyink, V. L., & Jenkins, D. (1980). *Water chemistry*: New York, John Wiley.

Stolpe, N. B., McCallister, D. L., Shea, P. J., Lewis, D. T., & Dam, R. (1993). Mobility of aniline, benzoic acid, and toluene in four soils and correlation with soil properties. *Environmental Pollution, 81*(3), 287-295. doi: http://dx.doi.org/10.1016/0269-7491(93)90211-6

Stumm, W., & Sulzberger, B. (1992). The cycling of iron in natural environments: Considerations based on laboratory studies of heterogeneous redox processes. *Geochimica et Cosmochimica Acta, 56*(8), 3233-3257. doi: http://dx.doi.org/10.1016/0016-7037(92)90301-X

Sung, W., & Morgan, J. J. (1980). Kinetics and product of ferrous iron oxygenation in aqueous systems. *Environmental science & technology, 14*(5), 561-568.

Sutton, H. C. (1985). Efficiency of chelated iron compounds as catalysts for the Haber-Weiss reaction. *Journal of free radicals in biology & medicine, 1*(3), 195-202.

Thirunavukkarasu, O., Viraraghavan, T., & Subramanian, K. (2003). Arsenic removal from drinking water using iron oxide-coated sand. *Water, air, and soil pollution, 142*(1-4), 95-111.

Vayssieres, L., Beermann, N., Lindquist, S.-E., & Hagfeldt, A. (2001). Controlled aqueous chemical growth of oriented three-dimensional crystalline nanorod arrays: application to iron (III) oxides. *Chemistry of materials, 13*(2), 233-235.

Wang, H., White, G., Dixon, J., & Turner, F. (1993). Ferrihydrite, lepidocrocite, and goethite in coatings from east Texas vertic soils. *Soil Science Society of America Journal, 57*(5), 1381-1386.

Wang, J. L., & Xu, L. J. (2012). Advanced oxidation processes for wastewater treatment: formation of hydroxyl radical and application. *Critical reviews in environmental science and technology, 42*(3), 251-325.

Wehrli, B., Sulzberger, B., & Stumm, W. (1989). Redox processes catalyzed by hydrous oxide surfaces. *Chemical Geology, 78*(3–4), 167-179. doi: http://dx.doi.org/10.1016/0009-2541(89)90056-9

Wells, C., & Salam, M. (1965). Hydrolysis of ferrous ions: a kinetic method for the determination of the Fe (II) species. *Nature,* 205, 690-692. doi:10.1038/205690b0

Wells, C., & Salam, M. (1968). The effect of pH on the kinetics of the reaction of iron (II) with hydrogen peroxide in perchlorate media. *Journal of the Chemical Society A: Inorganic, Physical, Theoretical*, 24-29.

Xu, Y., & Axe, L. (2005). Synthesis and characterization of iron oxide-coated silica and its effect on metal adsorption. *Journal of Colloid and Interface Science, 282*(1), 11-19. doi: http://dx.doi.org/10.1016/j.jcis.2004.08.057

Yeh, C. K.-J., Hsu, C.-Y., Chiu, C.-H., & Huang, K.-L. (2008). Reaction efficiencies and rate constants for the goethite-catalyzed Fenton-like reaction of NAPL-form aromatic hydrocarbons and chloroethylenes. *Journal of Hazardous Materials, 151*(2–3), 562-569. doi: http://dx.doi.org/10.1016/j.jhazmat.2007.06.014

Yuen, S., Kubsh, J., Dumesic, J., Topsøe, N., Topsøe, H., & Chen, Y. (1982). Metal oxide-support interactions in silica-supported iron oxide catalysts probed by nitric oxide adsorption. *The Journal of Physical Chemistry*, *86*(15), 3022-3032.

Zachara, J., Gassman, P., Smith, S., & Taylor, D. (1995). Oxidation and adsorption of Co (II) EDTA< sup> 2−</sup> complexes in subsurface materials with iron and manganese oxide grain coatings. *Geochimica et Cosmochimica Acta*, *59*(21), 4449-4463.

Zhang, W., Singh, P., Paling, E., & Delides, S. (2004). Arsenic removal from contaminated water by natural iron ores. *Minerals engineering*, *17*(4), 517-524.